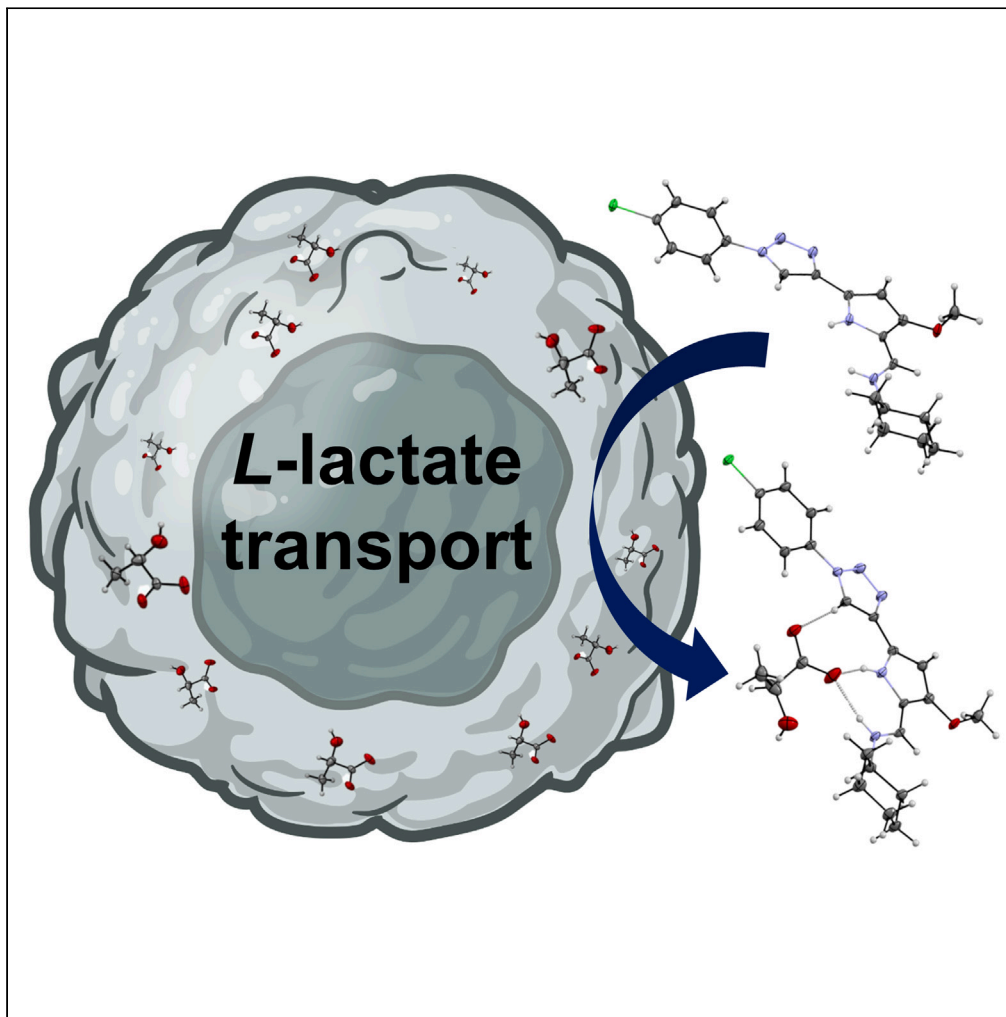**Article**

Small molecule anion carriers facilitate lactate transport in model liposomes and cells

Daniel Alonso-Carrillo, Alain Arias-Betancur, Israel Carreira-Barral, ..., María García-Valverde, Ricardo Pérez-Tomás, Roberto Quesada

rperez@ub.edu (R.P.-T.)
rquesada@ubu.es (R.Q.)

Highlights

Small molecules can facilitate L-lactate transport across phospholipid membranes

Observed lactate transport is independent from monocarboxylate transporters in cells

The most potent transporter showed an additive effect with CisPt in cancer cells

Article

Small molecule anion carriers facilitate lactate transport in model liposomes and cells

Daniel Alonso-Carrillo,[1,5] Alain Arias-Betancur,[2,3,4,5] Israel Carreira-Barral,[1] Pere Fontova,[1] Vanessa Soto-Cerrato,[2,3] María García-Valverde,[1] Ricardo Pérez-Tomás,[2,3,*] and Roberto Quesada[1,6,*]

SUMMARY

An excessive production of lactate by cancer cells fosters tumor growth and metastasis. Therefore, targeting lactate metabolism and transport offers a new therapeutic strategy against cancer, based on dependency of some cancer cells for lactate as energy fuel or as oncogenic signal. Herein we present a family of anionophores based on the structure of click-tambjamines that have proved to be extremely active lactate carriers across phospholipid membranes. Compound 1, the most potent lactate transmembrane carrier, was studied in HeLa cells. The use of a monocarboxylate transporters (MCTs) inhibitor proved that 1 is an active lactate transporter in living cells, confirming the results obtained in phospholipid vesicles. Moreover, an additive effect of compound 1 with cisplatin was observed in HeLa cells. Identification of active lactate anionophores working in living cells opens up ways to exploit this class of compounds as molecular tools and drugs addressing dysregulated lactate metabolism.

INTRODUCTION

Lactate (L-lactate) anion is the product of glycolysis and the major fuel for mitochondrial respiration,[1] as well as an intracellular signaling mediator.[2] In particular, tumor cells produce large amounts of this metabolite as a result of their abnormal metabolism, the so-called 'Warburg effect'.[3,4] Thus, lactate concentrations in cancer tissues are much higher (10–30 mM) than in healthy tissues (1.5–3 mM).[5,6] Lactate is a key regulator of cancer development,[7] and overproduction of lactate by cancer cells promotes tumor growth, immune escape, angiogenesis, metastasis and tumor drug resistance.[8] Intracellular lactate efflux is mediated by a family of transmembrane proteins named monocarboxylate transporters (MCTs). These MCTs facilitate lactate transport promoting lactate/H^+ symport, and intracellular lactate efflux leads to acidification of the tumor microenvironment (acidosis) and reversal of the pH gradient that exists in healthy cells.[9] Acidosis is a hallmark of cancer and MCTs are overexpressed in several types of cancers, such as breast, bone, colon and renal cancers.[10,11] Targeting abnormal lactate production and transport is a promising approach to cancer therapeutics.[12] In this regard, interfering lactate production through modulating glycolysis, like inhibiting lactate dehydrogenase, has been proposed.[13] Secondly, lactate shuttle modulation by inhibiting MCTs has been proven to inhibit the growth of cancer cells, intracellular acidification and reduction in migration of cancer cells, among others.[14] On this matter, clinical trials (phases I and II) are being carried out involving MCTs inhibitors, which prevent proliferation of cancer cells showing aggressive phenotypes.[15–17] Alternatively, a yet unexplored approach could be developing synthetic lactate carriers capable of facilitating lactate transport independently from naturally occurring MCTs. In this regard, small-molecule anion transporters are currently attracting significant interest.[18,19] Biological applications of these compounds are being explored, including anticancer, antibacterial and channel replacement therapies applications.[20–24] Most of these studies focus on chloride transport and the lactate anion has been largely neglected in transmembrane transport studies despite its biological relevance.[25] We have recently reported a new family of compounds, 'click-tambjamines', inspired by the structure of tambjamines alkaloids.[26] These molecules display a remarkable anionophoric activity both in model liposomes and cells.[27] These precedents, as well as the easy tunability of the design, prompted us to explore the activity of this class of compounds as L-lactate transporters both in liposomes and *in vitro*.

RESULTS AND DISCUSSION

Compounds and solid state studies

Compounds **1–6** were selected for this study, bearing a similar hydrogen-bonding cleft involving two N-H groups as well as a polarized C-H fragment of the 1,2,3-triazolyl heterocycle and different triazolyl and imine substituents (Figure 1A). Compound **6** was previously reported by us[26] and compounds **1–5** were selected to explore a family of compounds which could potentially cover a range of transport activities while

[1]Departamento de Química, Facultad de Ciencias, Universidad de Burgos, 09001 Burgos, Spain
[2]Department of Pathology and Experimental Therapeutics, Faculty of Medicine and Health Sciences, Universitat de Barcelona, L'Hospitalet de Llobregat, 08907, Spain
[3]Molecular Signalling, Oncobell Program, Institut d'Investigació Biomèdica de Bellvitge (IDIBELL), L'Hospitalet de Llobregat, 08908, Spain
[4]Department of Integral Adult Dentistry, Dental School, Research Centre for Dental Sciences, Universidad de La Frontera, Temuco 4811230, Chile
[5]These authors contributed equally
[6]Lead contact
*Correspondence: rperez@ub.edu (R.P.-T.), rquesada@ubu.es (R.Q.)
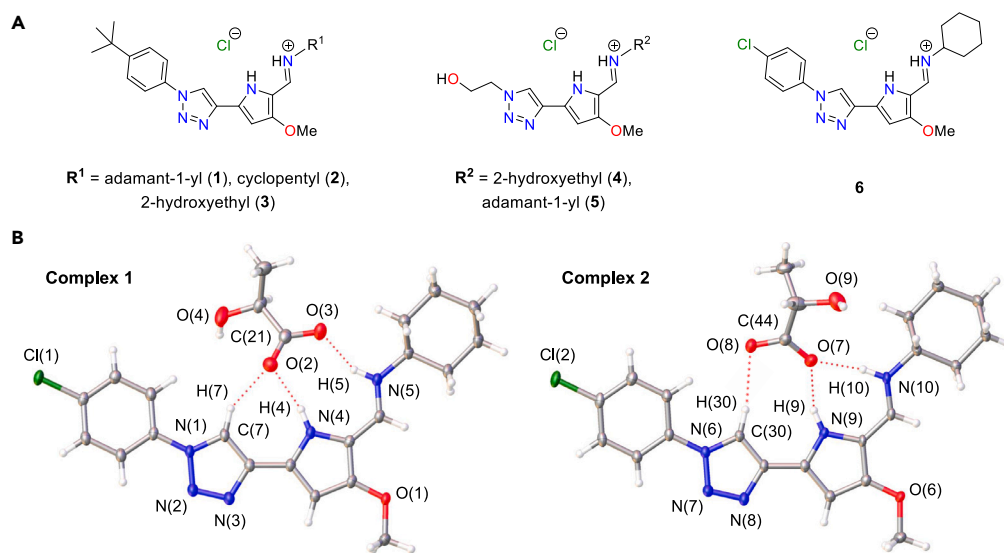https://doi.org/10.1016/j.isci.2023.107898

Figure 1. Synthesized compounds and crystal structure of 6.Lactate complex
(A) Structures of the studied compounds (**1–6**).
(B) X-ray structure of **6**·Lactate complex. The two complexes found in the asymmetric unit have been represented to highlight the receptor-lactate interactions.
Two crystallization water molecules have been omitted for the sake of simplicity. The Olex2 plot is at the 50% probability level.

conserving structural similarities. Compounds were obtained in moderate-good yields and isolated and fully characterized as hydrochloride salts (Figures S1–S27).

Evidence for the suitability of these compounds to coordinate lactate was obtained in the solid state. Single crystals suitable for X-ray diffraction analysis of the lactate adduct of **6** were grown by slow evaporation of a 2:1 methanol/n-butanol solution of compound **6** containing 2 equiv. of sodium L-lactate, the biologically relevant enantiomer of this anion. The asymmetric unit consists of two 1:1 receptor:lactate entities and two crystallization water molecules. In both complexes, the lactate anion interacts with the three hydrogen-bond donor groups of the click-tambjamine through its carboxylate group via hydrogen-bonding interactions, but in a different fashion depending on the complex (Figures 1B and S28; Table S1). For complex 1, one of the carboxylate's oxygen atoms interacts simultaneously with the triazole C-H [C(7)··· O(2) 2.981 Å, C(7)-H(7)···O(2) 148.59°] and pyrrole N-H [N(4)···O(2) 2.796 Å, N(4)-H(4)···O(2) 167.66°] fragments, whereas the other one establishes a hydrogen bond with the imine N-H group [N(5)···O(3) 2.697 Å, N(5)-H(5)···O(3) 149.07°]. In the case of complex 2 the situation is the reverse: one of the carboxylate's oxygen atoms interacts with the pyrrole [N(9)···O(7) 2.620 Å, N(9)-H(9)···O(7) 159.00°] and imine [N(10)···O(7) 2.757 Å, N(10)-H(10)···O(7) 169.30°] N-H fragments, with the other one forming a hydrogen bond with the triazole C-H group [C(30)···O(8) 3.250 Å, C(30)-H(30)···O(8) 164.93°]. Hydrogen-bonding interactions involving the triazole C-H are comparatively weaker than those involving the pyrrole and imine N-H, which is in agreement with the lower polarization of the C-H bond if compared with the N-H ones.[28] Each crystallization water molecule forms an array of hydrogen bonds (with another water molecule and two neighboring lactate anions, involving the lactate O-H group as well) that contributes to the overall stability of the structure. The click-tambjamine's core was found to be essentially flat, since the deviation from planarity of the plane defined by the atoms of the pyrrole and triazole rings and those from the imine subunit is, on average, 0.051 Å (mean value obtained considering the two complexes the asymmetric unit is comprised of).

Solution studies

The interaction of the synthesized compounds with the chloride anion in solution was investigated by means of ^{1}H NMR spectroscopy in DMSO-d_6. A concentrated solution of the corresponding hydrochloride salt was successively diluted and the spectra of the different solutions recorded (Figures S29–S42). Figure 2 shows the stack plot obtained for compound **1**. The signals corresponding to the pyrrole and imine N-H protons experience a remarkable downfield shift as the concentration of compound increases. Likewise, that of the triazole C-H proton undergoes a similar shift albeit to a lesser extent. This pattern, also observed for the other studied compounds, confirms the interaction of chloride with click-tambjamines through hydrogen bonds; such interaction is stronger with the N-H fragments than with the C-H group, as expected given the higher acidity of the former. To quantify the strength of this interaction, the shifts of the signals of the N-H protons and of the triazole C-H proton were plotted as a function of the concentration of compound, and the resulting profiles fitted simultaneously with the BindFit software to a 1:1 LH:Cl isotherm,[29,30] being LH the protonated host and Cl the guest, the chloride anion (see ESI). This provided the association constant (K_a) values, displayed in Table 1, which are similar for the six studied derivatives. This result suggests that, for compounds **3**, **4** and **5**, the O-H group/s does/do not cooperate in the binding of the chloride anion. Interestingly, these values resemble
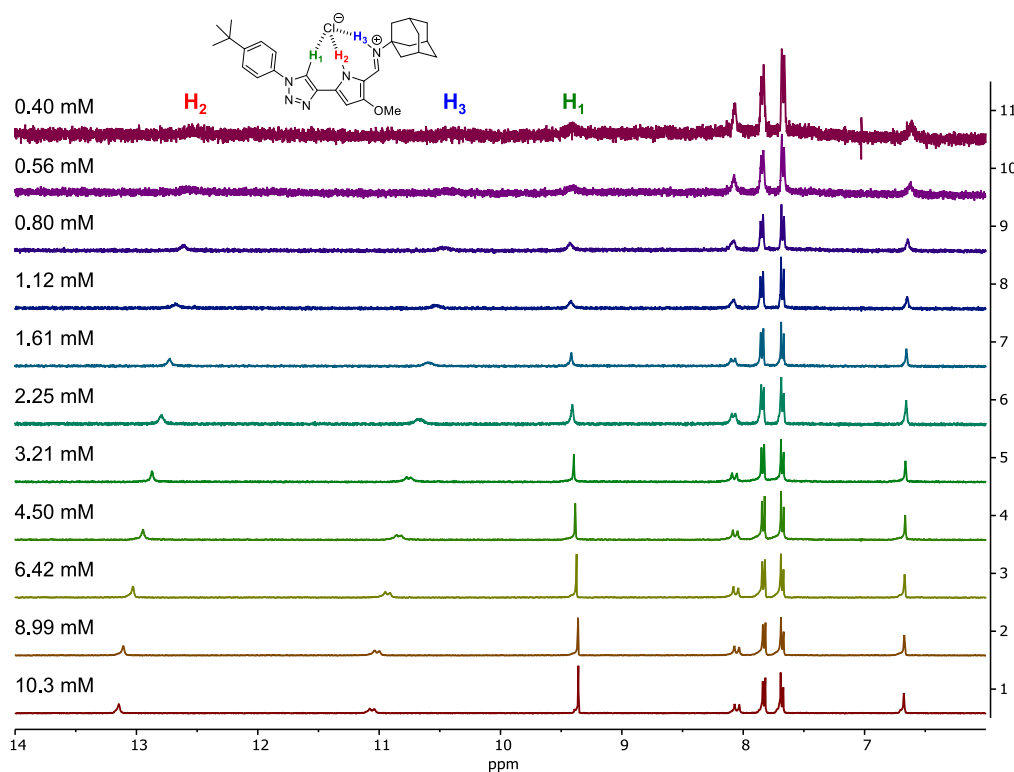
Figure 2. Chloride binding studies monitored by ^{1}H NMR spectroscopy
Stack plot of partial ^{1}H NMR spectra (400 MHz, 298 K) of compound **1**·HCl in DMSO-d_6, obtained by serial dilution of a 10.3 mM solution of the compound.

those previously reported by our research group for structurally related compounds, and also for compound **6**, although in that work a titration of the hydroperchloric salts with tetrabutylammonium chloride was performed.[26]

Transmembrane anion transport studies

Transmembrane anion transport experiments were conducted in model liposomes (1-palmitoyl-2-oleoyl-sn-glycero-3-phosphocoline, POPC) and monitored by potentiometric techniques (ion-selective electrode, ISE) and emission spectroscopy. For ISE assays, liposomes were loaded with a sodium chloride buffered aqueous solution and dispersed in an isotonic, chloride-free solution (see STAR Methods for details).[32] Chloride efflux promoted by the transporter was followed over time and referred to the total chloride concentration, which was ascertained after lysing liposomes with a surfactant; this was performed for several concentrations of transporter. Plotting the chloride efflux observed at each of these concentrations at 300 s against such concentrations and fitting the obtained profile to Hill's equation

Table 1. Association constants, transport activities, and calculated lipophilicities for the studied compounds

Code	K_a	EC_{50} Cl^-/NO_3^-	EC_{50} Cl^-/HCO_3^-	EC_{50} Cl^-/Lac^-	LogP[a]
1	217 ± 3	3.7 ± 0.4	39 ± 2	8 ± 1	5.74
2	235 ± 2	16 ± 1	138 ± 17	34 ± 4	4.71
3	128 ± 4	8340 ± 431	[b]	7659 ± 547	2.95
4	134 ± 1	n. d.	n. d.	n. d.	−0.55
5	219 ± 2	n. d.	n. d.	n. d.	2.40
6	294 ± 2	32.6 ± 0.8[c]	130 ± 7[c]	34 ± 4	4.22[c]

Association constants K_a (M^{-1}) calculated for the chloride adducts derived from the studied compounds (DMSO-d_6, 298 K), transport activities expressed as EC_{50} (nM) for the tested compounds, and calculated lipophilicities (logP).
[a]Determined for the deprotonated form of the compound through Virtual Computational Chemistry Laboratory as an average logP.[31]
[b]The carrier displays a moderate activity but no EC_{50} value could be calculated reliably. However, it can be estimated to be close to 15 μM.
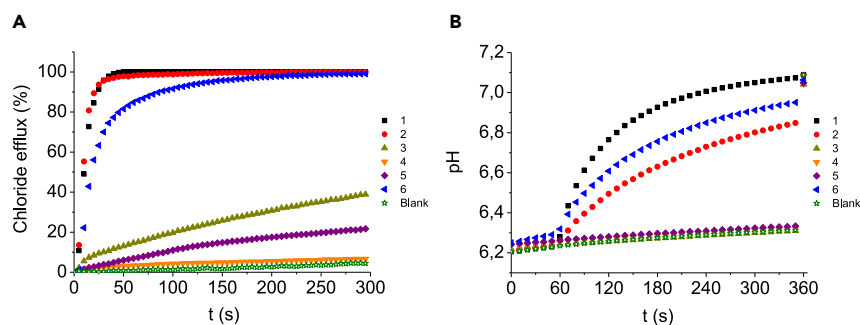[c]Data taken from ref.[26]

Figure 3. Transmembrane anion transport studies in model liposomes

(A) Chloride efflux promoted by the studied compounds (5 μM in all cases) or the blank (DMSO, 6.25 μL) in unilamellar POPC vesicles (0.5 mM POPC). Vesicles loaded with a NaCl aqueous solution (451 mM NaCl, 20 mM NaH_2PO_4, I.S. 500 mM, pH 7.2) were immersed in a Na_2SO_4/NaLac aqueous solution (150 mM Na_2SO_4, 40 mM NaLac, 20 mM NaH_2PO_4, I.S. 500 mM, pH 7.2). Each trace represents the average of at least three trials performed with three batches of vesicles.

(B) Variation of pH upon addition of the studied compounds to 7:3 POPC:cholesterol vesicles (0.5 mM POPC). Vesicles loaded with a $NaNO_3$ aqueous solution (126.2 mM $NaNO_3$, 10 mM NaH_2PO_4, 1 mM HPTS, I.S. 150 mM, pH 6.2) were suspended in a $NaNO_3$ aqueous solution (126.2 mM $NaNO_3$, 10 mM NaH_2PO_4, I.S. 150 mM, pH 7.5) just before starting the measurements. At t = 60 s the compound (0.5 nM, 0.0001% mol carrier to lipid concentration) or the blank (DMSO, 6.25 μL) was added, and at t = 360 s a detergent (Triton™ X-100, 20% dispersion in water, 20 μL) was added. Each trace corresponds to the average of at least three trials performed with three batches of vesicles.

provided EC_{50}, the concentration of compound required to elicit 50% chloride efflux, and the Hill parameter, *n*, representing the number of molecules of transporter per anion. The lower the value of the EC_{50} parameter, the more potent the compound is. This experiment was carried out using different anions in the outer milieu of liposomes: nitrate, bicarbonate, L-lactate and sulfate. In all cases, the observed chloride efflux is the result of the exchange of this encapsulated anion by the extravesicular anion. The results are presented in Table 1 (see Table S2 for more details). Figure 3A shows the chloride efflux induced by compounds **1–6** when lactate was outside the liposomes (see Figures S43–S74 for more details).

Variation of EC_{50} parameter when investigating the chloride efflux in the presence of external nitrate, bicarbonate or L-lactate is consistent with anion exchange (antiport) as the main mechanism accounting for the transport activity displayed by these anionophores. Such activity clearly depends on the nature of the triazole and imine's substituents. The order of activity was found to be **1** > **2–6** ≫ **3**, **4** and **5**. Derivatives **1**, **2** and **6**, with aromatic and alicyclic fragments linked to the triazole and imine subunits, respectively, are extremely active, with EC_{50} values in the low nanomolar range. On the contrary, those bearing one (**3** and **5**) or two (**4**) 2-hydroxyethyl substituents showed a dramatic drop on their activity to the point of preventing the calculation of reliable EC_{50} values in most of the cases. The presence of this residue reduces the lipophilicity of these molecules significantly, an effect that is well known to result in lowering the activity exhibited by these derivatives.[33] For the highly active **1**, **2** and **6**, the smallest EC_{50} values were obtained for the Cl^-/NO_3^- exchange assay followed by those determined for the Cl^-/Lac^- and Cl^-/HCO_3^- exchange assays. In addition to the remarkable lactate transport activity observed, these compounds are more active transporting this anion than bicarbonate, with EC_{50} values roughly 4–5 times smaller for lactate. Overall, compound **1** stands out as the most potent compound in these assays.

The ability of compounds **1–6** to dissipate pH gradients was also examined employing the HPTS transport assay.[34] 7:3 POPC:cholesterol liposomes were hydrated with a sodium nitrate buffered aqueous solution containing the ratiometric fluorescent probe HPTS (pH 6.2), which is sensitive to pH changes, and suspended in an isotonic sodium nitrate aqueous solution (pH 7.5). Changes in the I_{460}/I_{403} ratio were followed upon addition of the compounds and, after 300 s, liposomes were lysed with a detergent; emission changes were subsequently converted into pH values through calibration (Figure S82). The observed results were similar to those discussed in ISE assays. Compounds **1**, **2** and **6** were found to be extremely active, whereas derivatives **3**, **4** and **5** displayed very limited activities (Figure 3B). Concentration-dependent experiments (Figures S83–S88) indicate that the active **1**, **2** and **6** are able to discharge the 1.3 units pH gradient at a concentration as low as 0.5 nM, with **1** displaying again the highest activity. Fluorescence assays employing entrapped lucigenin to detect lactate transport facilitated by these compounds were also carried out (Figures S89–S96). The results support again the activity trends described above.

To rule out the possibility of these compounds inducing large non-selective pores in the membrane, carboxyfluorescein leakage experiments were also conducted (Figures S75–S81). In all cases, the performed assays confirm that none of these compounds behaves as a detergent, and therefore their anionophoric activity is due exclusively to their ability to transport anions across the membrane.

In order to obtain a direct evidence of lactate transport in model vesicles ^{13}C NMR spectroscopy experiments were performed. The experiment is illustrated in Figure 4. POPC liposomes filled with sodium L-lactate-1-^{13}C were prepared and suspended in an isotonic lactate-free medium. Addition of a NaCl pulse in the presence of active lactate transporter **1** facilitates lactate efflux from the interior of the vesicles. The signal of this extravesicular lactate can be broadened by addition of paramagnetic $MnCl_2$ (Figure 4C **left**). Addition of $MnCl_2$ to a control experiment in which compound **4** is used resulted in no changes because the encapsulated L-lactate-1-^{13}C is not affected by extravesicular $MnCl_2$ (Figure 4C **right**).

Overall, this set of experiments confirmed the identification of **1**, **2** and **6** as potent lactate transporters in model vesicles.
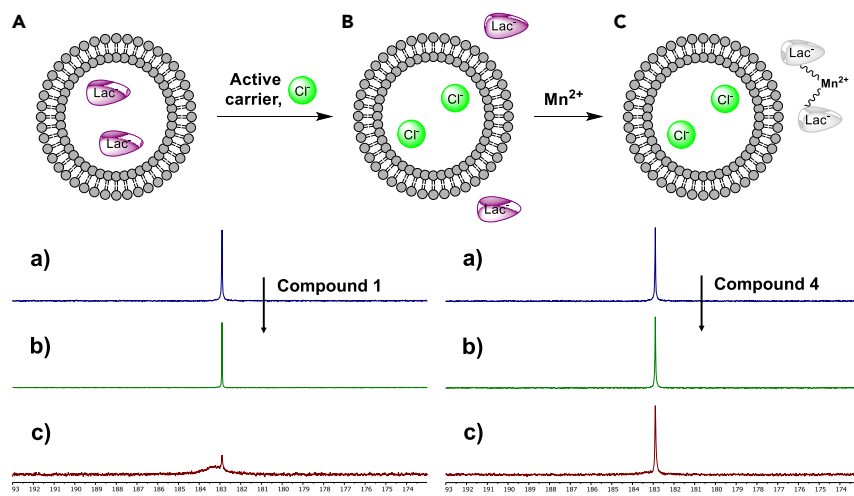
Figure 4. Lactate transport in model liposomes monitored by ^{13}C NMR spectroscopy

(A) ^{13}C NMR spectra (500 MHz, D$_2$O) evidencing the facilitated chloride/lactate exchange: a) POPC vesicles loaded with a CH$_3$CH(OH)^{13}CO$_2$Na aqueous solution (200 mM labeled NaLac, 20 mM NaH$_2$PO$_4$, pH 7.2) dispersed in a lactate-free aqueous solution (150 mM Na$_2$SO$_4$, 20 mM NaH$_2$PO$_4$, pH 7.2).

(B) After addition of a NaCl aqueous solution (50 mM NaCl in the experiment) and **1** (the active carrier, left) or **4** (the non-active carrier, right) (1% mol carrier to lipid concentration in both cases).

(C) After addition of a MnCl$_2$ aqueous solution (0.5 mM MnCl$_2$ in the experiment), a paramagnetic reagent affecting only extravesicular CH$_3$CH(OH)^{13}CO$_2^-$ anions.

Biological studies

First, the cytotoxicity of compounds **1–6** was analyzed. The inhibitory concentrations that cause 25, 50 and 75% growth inhibition (IC values) at 24 h were determined on several cancer cell lines: cervix and breast adenocarcinoma cell lines (HeLa and MCF7, respectively), oral squamous carcinoma cell line (CAL27), and non-cancer epithelial breast cell line (MCF10A) (Table 2). A reasonably good correlation between cytotoxicity and potency as transmembrane anion carriers was found for this series of compounds, suggesting a correlation between these properties.

Table 2. IC values of the studied compounds in different cell lines

Code	IC	HeLa	CAL27	MCF7	MCF10A
1	IC$_{75}$	3.95 ± 0.26	4.00 ± 0.50	7.91 ± 1.42	11.22 ± 3.94
	IC$_{50}$	3.36 ± 0.19	3.27 ± 0.27	5.58 ± 1.17	7.66 ± 1.86
	IC$_{25}$	2.85 ± 0.16	2.68 ± 0.18	4.00 ± 1.22	5.36 ± 1.09
2	IC$_{75}$	13.77 ± 1.88	12.35 ± 2.40	20.49 ± 3.88	25.65 ± 3.97
	IC$_{50}$	12.48 ± 0.98	10.64 ± 2.06	9.06 ± 2.35	18.68 ± 2.55
	IC$_{25}$	11.34 ± 0.38	9.25 ± 2.26	4.04 ± 1.37	13.62 ± 1.64
3	IC$_{75}$	15.29 ± 1.87	20.88 ± 4.45	34.69 ± 3.11	35.95 ± 4.27
	IC$_{50}$	13.52 ± 1.05	17.41 ± 3.31	15.79 ± 1.14	25.36 ± 1.61
	IC$_{25}$	11.98 ± 0.40	14.62 ± 3.20	7.22 ± 0.85	18.11 ± 3.23
4	IC$_{75}$	>100	>100	>100	>100
	IC$_{50}$	>100	82.12 ± 2.88	>100	>100
	IC$_{25}$	>100	60.97 ± 5.40	>100	98.64 ± 0.94
5	IC$_{75}$	93.73 ± 3.71	>100	>100	>100
	IC$_{50}$	85.57 ± 2.94	95.99 ± 4.79	>100	>100
	IC$_{25}$	78.14 ± 3.00	86.88 ± 6.79	>100	94.92 ± 5.23
6	IC$_{75}$	6.54 ± 0.02	8.44 ± 2.59	14.53 ± 1.23	6.12 ± 1.56
	IC$_{50}$	6.31 ± 0.06	7.41 ± 2.77	11.46 ± 1.19	4.61 ± 0.15
	IC$_{25}$	6.09 ± 0.09	6.58 ± 2.98	9.05 ± 1.13	3.49 ± 0.22

IC values of compounds **1–6** in HeLa, CAL27, MCF7, and MCF10A cell lines. Values are presented as mean ± SD in μM. All the assays were performed in triplicate and results were obtained from at least three independent experiments.
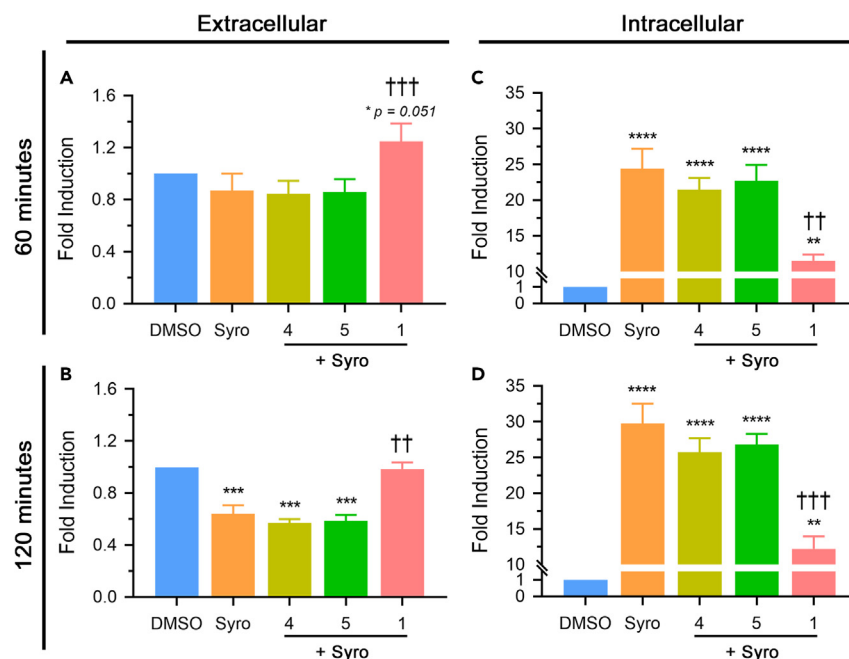
Figure 5. Lactate transport assays in HeLa cells

(A–D) Lactate transport experiments in HeLa cells treated with **1**, **4**, **5** (3.9 μM), Syro and DMSO for 60 and 120 min. Extracellular (A and B) and intracellular (C and D) lactate levels are expressed as fold of change regarding DMSO. Syro was used for MCT inhibition (10 μM, 1 h before **1**, **4** or **5**). Each experiment was performed at least three times and bars represent mean ± SEM. One-way ANOVA was performed and statistical differences are indicated as follows: **p < 0.01, ***p < 0.001, and ****p < 0.0001 for comparison with DMSO; ††p < 0.01, and †††p < 0.001 for comparison with Syro.

Compound **1** displayed the highest cytotoxic effect, with IC_{50} values among different cell lines in the 3.3–7.7 μM range, whereas compounds **4** and **5** induced little cytotoxicity, either not reducing cell viability in most cell lines (IC_{50} value >100 μM) or showing high IC_{50} values (>82 μM). Derivatives **2**, **3** and **6** displayed a lower cytotoxicity than **1** (IC_{50} ranging from 4.6 to 25.4 μM), being **3** the only compound showing moderate cytotoxicity despite being an inefficient anionophore.

Considering both performance in transmembrane anion transport studies as well as cytotoxicity results, compound **1** was selected as candidate to explore its ability to transport lactate anions across cell membranes in HeLa cells, a highly glycolytic cancer cell line. Likewise, in addition to DMSO, **4** and **5** were used as negative controls for lactate transport. The determined IC_{75} concentration at 24 h of **1** (3.9 μM) was selected to study the extra- and intracellular lactate concentrations after 60 and 120 min of treatment with the different compounds, when no affectation on cell viability is observed, by using a luminescent-based method (Lactate-Glo Assay Kit, Promega, WI, USA). In regular culture conditions with high glucose medium, cancer cells export lactate (mainly produced by glycolysis) to the extracellular matrix through MCTs. Thus, in order to evaluate the activity of **1** as a lactate transporter in cells, MCT dual inhibitor (MCT1/MCT4) Syrosingopine (Syro) was used in the assays. Extra- and intracellular lactate levels are presented in Figure 5 as a fold of change compared to DMSO treatment. Firstly, as expected, upon treatment with Syro alone extracellular lactate levels were lower compared to controls treated with DMSO, achieving significant differences after 120 min (p < 0.001) (Figures 5A and 5B). In accordance, intracellular lactate levels after Syro treatment were significantly higher than DMSO at both 60 and 120 min of treatment (p < 0.0001) (Figures 5C and 5D). This result confirmed that Syro was able to impair lactate exportation via MCT inhibition, reducing extracellular lactate levels and, therefore, increasing intracellular lactate concentrations. Similarly, both extra- and intracellular lactate levels after treatment with **4** and **5** in the presence of Syro were similar to those with Syro alone, with no significant differences, confirming their lack of effect as lactate transporters in cells.

Secondly, upon treatment with **1** in the presence of Syro the consequences of MCTs inhibition were clearly ameliorated. At both 60 and 120 min, extracellular lactate levels of cells treated with **1** and pre-treated with Syro were similar to DMSO condition and significantly higher than levels observed after treatment with Syro alone (p < 0.01) or with **4** and **5** in the presence of Syro (Figures 5A and 5B). Moreover, at both 60 and 120 min, after treatment with **1** in the presence of Syro, intracellular lactate levels were significantly lower, around 50% (p < 0.01 and p < 0.001, respectively), compared with Syro alone or with **4** and **5** pre-treated with Syro (Figures 5C and 5D). Altogether, these results confirm that **1** functions as lactate transporter in cells, being able to partially revert the effect of intracellular lactate accumulation caused by MCTs inhibition, mediated by Syro, and favoring lactate exportation from the intracellular compartment to the extracellular space.

Finally, the ability of **1** to sensitize cancer cells against first-line standard chemotherapy cisplatin (CisPt) was assessed in HeLa cells through the MTT assay. In a sequential combination, cells were treated with **1** (using IC_{10}, IC_{25}, IC_{50} and IC_{75} values) for 24 h and then CisPt was added for additional 24 h at different doses. Results showed that the effect of the combination therapy on cell viability was higher compared with respective monotherapy of CisPt (Figure 6A) for all the doses of **1** tested.
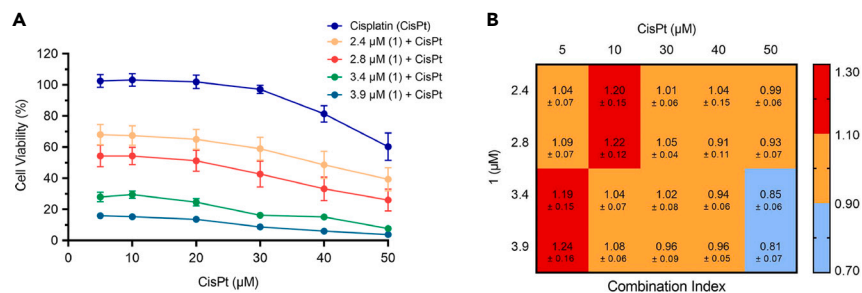
Figure 6. Combination therapy for 1 and CisPt in HeLa cells

(A) Cell viability percentages after 24 h of treatment with CisPt monotherapy (5–50 μM) and the combination of **1** (IC_{10}, IC_{25}, IC_{50} and IC_{75} values) and CisPt (24 h each sequentially). Bars represent mean ± SEM.

(B) Analysis of synergy between **1** and CisPt through determination of Combination Index (CI) in the same conditions as in (A). Data represent averages of three independent experiments.

The percentages of cell population affected by the combination therapy were analyzed with CompuSyn software (version 1.0; ComboSyn, Paramus, NJ, USA) to determine the Combination Index (CI) for the different dose combination. CI is used to describe the type of interaction between therapeutic compounds and according to the value the combination can be synergic (0.30 < CI < 0.70), moderate synergic (0.70 < CI < 0.85), slight synergic (0.85 < CI < 0.90), additive (0.90 < CI < 1.10) and antagonist (CI > 1.10).[35] The results showed that for the majority of the dose combinations tested there was an additive effect whereas a moderate synergic effect was observed when higher doses of both **1** and CisPt were combined (Figure 6B).

Conclusions

We have demonstrated here the possibility of facilitating the transmembrane transport of L-lactate by anionophores based on the structure of click-tambjamines. The hydrogen-bonding cleft displayed by these compounds is well suited to interact with this anion as evidenced by the solid state structure of the **6·Lac** complex. Several anionophores showed excellent transport efficiency in model liposomes at nanomolar concentrations, and the ability of the most potent carrier, compound **1**, to promote lactate transport was also assayed in HeLa cells. Inhibiting the activity of MCTs by using Syrosingopine, allowed us to demonstrate that **1** is able to facilitate lactate transport in living cells independently of MCTs activity. We have also shown that **1** showed an additive effect with first-line standard chemotherapy CisPt in cancer cells. This makes **1** a promising drug to be used in a therapy addressing dysregulated lactate metabolism. Investigations to decipher the biological applications of synthetic lactate transporters are currently underway in our laboratories.

Limitations of the study

The work presented here represents a proof of principle showing the ability of small molecules of facilitating lactate transport in both model vesicles and cells. An extended screening involving different types of anionophores will allow structure activity relationships studies to identify the most potent derivatives and the parameters governing this activity. Biological studies to understand the effect of facilitated lactate transport in living cells at the molecular level are needed to evaluate the potential applications of these compounds.

STAR★METHODS

Detailed methods are provided in the online version of this paper and include the following:

- KEY RESOURCES TABLE
- RESOURCE AVAILABILITY
  - Lead contact
  - Materials availability
  - Data and code availability
- EXPERIMENTAL MODEL AND STUDY PARTICIPANT DETAILS
  - Cellular models
- METHOD DETAILS
  - Synthesis and characterisation of compounds
  - X-ray diffraction studies
  - ^{1}H-NMR binding studies
  - Transmembrane anion transport experiments
  - Biological assays
- QUANTIFICATION AND STATISTICAL ANALYSIS

REFERENCES

1. Brooks, G.A. (2020). Lactate as a fulcrum of metabolism. Redox Biol. 35, 101454. https://doi.org/10.1016/j.redox.2020.101454.

2. Baltazar, F., Afonso, J., Costa, M., and Granja, S. (2020). Lactate beyond a waste metabolite: metabolic affairs and signaling in malignancy. Front. Oncol. 10, 231. https://doi.org/10.3389/fonc.2020.00231.

3. Parks, S.K., Mueller-Klieser, W., and Pouysségur, J. (2020). Lactate and acidity in the cancer microenvironment. Annu. Rev. Cancer Biol. 4, 141–158. https://doi.org/10.1146/annurev-cancerbio-030419-033556.

4. Warburg, O., Wind, F., and Negelein, E. (1927). The metabolism of tumors in the body. J. Gen. Physiol. 8, 519–530. https://doi.org/10.1085/jgp.8.6.519.

5. Walenta, S., Wetterling, M., Lehrke, M., Schwickert, G., Sundfør, K., Rofstad, E.K., and Mueller-Klieser, W. (2000). High lactate levels predict likelihood of metastases, tumor recurrence, and restricted patient survival in human cervical cancers. Cancer Res. 60, 916–921.

6. Brizel, D.M., Schroeder, T., Scher, R.L., Walenta, S., Clough, R.W., Dewhirst, M.W., and Mueller-Klieser, W. (2001). Elevated tumor lactate concentrations predict for an increased risk of metastases in head-and-neck cancer. Int. J. Radiat. Oncol. Biol. Phys. 51, 349–353. https://doi.org/10.1016/S0360-3016(01)01630-3.

7. Doherty, J.R., and Cleveland, J.L. (2013). Targeting lactate metabolism for cancer therapeutics. J. Clin. Invest. 123, 3685–3692. https://doi.org/10.1172/JCI69741.

8. Feichtinger, R.G., and Lang, R. (2019). Targeting L-lactate metabolism to overcome resistance to immune therapy of melanoma and other tumor entities. J. Oncol. 2019, 2084195. https://doi.org/10.1155/2019/2084195.

9. Swietach, P., Vaughan-Jones, R.D., Harris, A.L., and Hulikova, A. (2014). The chemistry, physiology and pathology of pH in cancer. Phil. Trans. R. Soc. B 369, 20130099. https://doi.org/10.1098/rstb.2013.0099.

10. Felmlee, M.A., Jones, R.S., Rodriguez-Cruz, V., Follman, K.E., and Morris, M.E. (2020). Monocarboxylate transporters (SLC16): function, regulation, and role in health and disease. Pharmacol. Rev. 72, 466–485. https://doi.org/10.1124/pr.119.018762.

11. Park, S.J., Smith, C.P., Wilbur, R.R., Cain, C.P., Kallu, S.R., Valasapalli, S., Sahoo, A., Guda, M.R., Tsung, A.J., and Velpula, K.K. (2018). An overview of MCT1 and MCT4 in GBM: small molecule transporters with large implications. Am. J. Cancer Res. 8, 1967–1976.

12. Pérez-Tomás, R., and Pérez-Guillén, I. (2020). Lactate in the tumor microenvironment: an essential molecule in cancer progression and treatment. Cancers 12, 3244. https://doi.org/10.3390/cancers12113244.

13. de la Cruz-López, K.G., Castro-Muñoz, L.J., Reyes-Hernández, D.O., García-Carrancá, A., and Manzo-Merino, J. (2019). Lactate in the regulation of tumor microenvironment and therapeutic approaches. Front. Oncol. 9, 1143. https://doi.org/10.3389/fonc.2019.01143.

14. Morais-Santos, F., Granja, S., Miranda-Gonçalves, V., Moreira, A.H.J., Queirós, S., Vilaça, J.L., Schmitt, F.C., Longatto-Filho, A., Paredes, J., Baltazar, F., and Pinheiro, C. (2015). Targeting lactate transport suppresses in vivo breast tumour growth. Oncotarget 6, 19177–19189. https://doi.org/10.18632/oncotarget.3910.

15. Guan, X., Rodriguez-Cruz, V., and Morris, M.E. (2019). Cellular uptake of MCT1 inhibitors AR-C155858 and AZD3965 and their effects on MCT-mediated transport of L-lactate in murine 4T1 breast tumor cancer cells. AAPS J. 21, 13. https://doi.org/10.1208/s12248-018-0279-5.

16. Polański, R., Hodgkinson, C.L., Fusi, A., Nonaka, D., Priest, L., Kelly, P., Trapani, F., Bishop, P.W., White, A., Critchlow, S.E., et al. (2014). Activity of the monocarboxylate transporter 1 inhibitor AZD3965 in small cell lung cancer. Clin. Cancer Res. 20, 926–937. https://doi.org/10.1158/1078-0432.CCR-13-2270.

17. Doherty, J.R., Yang, C., Scott, K.E.N., Cameron, M.D., Fallahi, M., Li, W., Hall, M.A., Amelio, A.L., Mishra, J.K., Li, F., et al. (2014). Blocking lactate export by inhibiting the myc target MCT1 disables glycolysis and glutathione synthesis. Cancer Res. 74, 908–920. https://doi.org/10.1158/0008-5472.CAN-13-2034.

18. Davis, J.T., Gale, P.A., and Quesada, R. (2020). Advances in anion transport and supramolecular medicinal chemistry. Chem. Soc. Rev. 49, 6056–6086. https://doi.org/10.1039/C9CS00662A.

19. Akhtar, N., Biswas, O., and Manna, D. (2020). Biological applications of synthetic anion transporters. Chem. Commun. 56, 14137–14153. https://doi.org/10.1039/D0CC05489E.

20. Yang, J., Chen, X., Xu, H., Shin, I., Gale, P.A., and Huang, F. (2021). Artificial transmembrane ion transporters as potential therapeutics. Chem 17, 3256–3259. https://doi.org/10.1016/j.chempr.2021.10.028.

21. Picci, G., Marchesan, S., and Caltagirone, C. (2022). Ion channels and transporters as therapeutic agents: from biomolecules to supramolecular medicinal chemistry. Biomedicines 10, 885. https://doi.org/10.3390/biomedicines10040885.

22. Roy, A., and Talukdar, P. (2021). Recent advances in bioactive artificial ionophores. ChemBioChem 22, 2925–2940. https://doi.org/10.1002/cbic.202100112.

23. Carreira-Barral, I., Rumbo, C., Mielczarek, M., Alonso-Carrillo, D., Herran, E., Pastor, M., Del Pozo, A., García-Valverde, M., and Quesada, R. (2019). Small molecule anion transporters display in vitro antimicrobial activity against clinically relevant bacterial strains. Chem. Commun. 55, 10080–10083. https://doi.org/10.1039/C9CC04304G.

24. Fiore, M., Cossu, C., Capurro, V., Picco, C., Ludovico, A., Mielczarek, M., Carreira-Barral, I., Caci, E., Baroni, D., Quesada, R., and Moran, O. (2019). Small molecule-facilitated anion transporters in cells for a novel therapeutic approach to cystic fibrosis. Br. J. Pharmacol. 176, 1764–1779. https://doi.org/10.1111/bph.14649.

25. Haynes, C.J.E., Berry, S.N., Garric, J., Herniman, J., Hiscock, J.R., Kirby, I.L., Light, M.E., Perkes, G., and Gale, P.A. (2013). Small neutral molecular carriers for selective carboxylate transport. Chem. Commun. 49, 246–248. https://doi.org/10.1039/C2CC37468D.

26. Carreira-Barral, I., Mielczarek, M., Alonso-Carrillo, D., Capurro, V., Soto-Cerrato, V., Pérez Tomás, R., Caci, E., García-Valverde, M., and Quesada, R. (2020). Click-tambjamines as efficient and tunable bioactive anion transporters. Chem. Commun. 56, 3218–3221. https://doi.org/10.1039/D0CC00643B.

27. Molero-Valenzuela, A., Fontova, P., Alonso-Carrillo, D., Carreira-Barral, I., Torres, A.A., García-Valverde, M., Benítez-García, C., Pérez-Tomás, R., Quesada, R., and Soto-Cerrato, V. (2022). A novel late-stage autophagy inhibitor that efficiently targets lysosomes inducing potent cytotoxic and sensitizing effects in lung cancer. Cancers 14, 3387. https://doi.org/10.3390/cancers14143387.

28. Hua, Y., and Flood, A.H. (2010). Click chemistry generates privileged CH hydrogen-bonding triazoles: the latest addition to anion supramolecular chemistry. Chem. Soc. Rev. 39, 1262–1271. https://doi.org/10.1039/B818033B.

29. Thordarson, P. (2011). Determining association constants from titration experiments in supramolecular chemistry. Chem. Soc. Rev. 40, 1305–1323. https://doi.org/10.1039/C0CS00062K.

30. www.supramolecular.org.

31. www.vcclab.org.

32. Jowett, L.A., and Gale, P.A. (2019). Supramolecular methods: the chloride/nitrate transmembrane exchange assay. Supramol. Chem. 31, 297–312. https://doi.org/10.1080/10610278.2019.1574017.

33. Knight, N.J., Hernando, E., Haynes, C.J.E., Busschaert, N., Clarke, H.J., Takimoto, K., García-Valverde, M., Frey, J.G., Quesada, R., and Gale, P.A. (2016). QSAR analysis of substituent effects on tambjamine anion transporters. Chem. Sci. 7, 1600–1608. https://doi.org/10.1039/C5SC03932K.

34. Gilchrist, A.M., Wang, P., Carreira-Barral, I., Alonso-Carrillo, D., Wu, X., Quesada, R., and Gale, P.A. (2021). Supramolecular methods: the 8-hydroxypyrene-1,3,6-trisulfonic acid (HPTS) transport assay. Supramol. Chem. 33, 325–344. https://doi.org/10.1080/10610278.2021.1999956.

35. Chou, T.-C. (2010). Drug combination studies and their synergy quantification using the Chou-Talalay method. Cancer Res. 70, 440–446. https://doi.org/10.1158/0008-5472.CAN-09-1947.

36. Hernando, E., Capurro, V., Cossu, C., Fiore, M., García-Valverde, M., Soto-Cerrato, V., Pérez-Tomás, R., Moran, O., Zegarra-Moran, O., and Quesada, R. (2018). Small molecule anionophores promote transmembrane anion permeation matching CFTR activity. Sci. Rep. 8, 2608. https://doi.org/10.1038/s41598-018-20708-3.

37. Sane, P.S., Tawade, B.V., Palaskar, D.V., Menon, S.K., and Wadgaonkar, P.P. (2012). Aromatic aldehyde functionalized polycaprolactone and polystyrene macromonomers: synthesis, characterization and aldehyde-aminiooxy click reaction. React. Funct. Polym. 72, 713–721. https://doi.org/10.1016/j.reactfunctpolym.2012.06.020.

38. Krause, L., Herbst-Irmer, R., Sheldrick, G.M., Stalke, D., and Stalke, D. (2015). Comparison of silver and molybdenum microfocus X-ray sources for single-crystal structure determination. J. Appl. Cryst. 48, 3–10. https://doi.org/10.1107/S1600576714022985.

39. Sheldrick, G.M. (2008). A short history of SHELX. Acta Cryst A64, 112–122. https://doi.org/10.1107/S0108767307043930.

40. Dolomanov, O.V., Bourhis, L.J., Gildea, R.J., Howard, J.A.K., Puschmann, H., and Puschmann, H. (2009). OLEX2: a complete structure solution, refinement and analysis program. J. Appl. Cryst. 42, 339–341. https://doi.org/10.1107/S0021889808042726.

41. Sheldrick, G.M. (2015). SHELXT – Integrated space-group and crystal-structure determination. Acta Cryst A71, 3–8. https://doi.org/10.1107/S2053273314026370.

STAR★METHODS

KEY RESOURCES TABLE

REAGENT or RESOURCE	SOURCE	IDENTIFIER
Chemicals, peptides, and recombinant proteins		
Chloroform	Carlo Erba Reagents	CAS Nº 67-66-3
Chloroform-d	VWR International	CAS Nº 865-49-6
Cholesterol	Merck – Sigma-Aldrich	CAS Nº 57-88-5
Copper(II) sulfate pentahydrate	Merck – Sigma-Aldrich	CAS Nº 7758-99-8
Cyclopentylamine	Alfa Aesar (Thermo Fisher Scientific)	CAS Nº 1003-03-8
Deuterium oxide	VWR International	CAS Nº 7789-20-0
Dichloromethane	Carlo Erba Reagents	CAS Nº 75-09-2
Diethyl ether	Carlo Erba Reagents	CAS Nº 60-29-7
Dimethyl sulfoxide-d_6	VWR International	CAS Nº 2206-27-1
Ethanolamine	Merck – Sigma-Aldrich	CAS Nº 141-43-5
Ethyl acetate	Carlo Erba Reagents	CAS Nº 141-78-6
Glacial acetic acid	Scharlau	CAS Nº 64-19-7
Hydrochloric acid (37%)	Scharlau	CAS Nº 7647-01-0
Lucigenin	Merck – Sigma-Aldrich	CAS Nº 2315-97-1
Manganese(II) chloride	Merck – Sigma-Aldrich	CAS Nº 7773-01-5
Methanol	Carlo Erba Reagents	CAS Nº 67-56-1
n-Butanol	Alfa Aesar (Thermo Fisher Scientific)	CAS Nº 71-36-3
n-Hexane	Carlo Erba Reagents	CAS Nº 110-54-3
Sephadex® G-25 (Medium)	Merck – Sigma-Aldrich	CAS Nº 9041-35-4
Sodium azide	Merck – Sigma-Aldrich	CAS Nº 26628-22-8
Sodium chloride	Merck	CAS Nº 7647-14-5
Sodium dihydrogen phosphate monohydrate	Merck	CAS Nº 10049-21-5
Sodium hydrogen carbonate	VWR International	CAS Nº 144-55-8
Sodium hydroxide	Scharlau	CAS Nº 1310-73-2
Sodium-L-ascorbate	Merck – Sigma-Aldrich	CAS Nº 134-03-2
Sodium L-lactate	PanReac AppliChem	CAS Nº 867-56-1
Sodium L-lactate-1-^{13}C solution	Merck – Sigma-Aldrich	CAS Nº 81273-81-6
Sodium nitrate	Scharlau	CAS Nº 7631-99-4
Sodium nitrite	Cymit Química	CAS Nº 7632-00-0
Sodium sulfate	Scharlau	CAS Nº 7757-82-6
tert-Butanol	Alfa Aesar (Thermo Fisher Scientific)	CAS Nº 75-65-0
Tetrabutylammonium hydroxide 30-hydrate	Acros Organics (Thermo Fisher Scientific)	CAS Nº 147741-30-8
Triton™ X-100	Merck – Sigma-Aldrich	CAS Nº 9036-19-5
1-Adamantylamine	BLDpharm	CAS Nº 768-94-5
1-Palmitoyl-2-oleoyl-sn-glycero-3-phosphocoline (POPC)	Merck – Sigma-Aldrich	CAS Nº 26853-31-6
2-Chloroethanol	Merck – Sigma-Aldrich	CAS Nº 107-07-3
4-(tert-Butyl)aniline	Alfa Aesar (Thermo Fisher Scientific)	CAS Nº 769-92-6
5(6)-Carboxyfluorescein	Thermo Fisher Scientific	CAS Nº 72088-94-9
8-Hydroxypyrene-1,3,6-trisulfonic acid trisodium salt (HPTS)	Alfa Aesar (Thermo Fisher Scientific)	CAS Nº 6358-69-6
5-Ethynyl-3-methoxy-1H-pyrrole-2-carbaldehyde	Faculty of Sciences, University of Burgos	
1-Azido-4-(tert-butyl)benzene (A1)	This Manuscript	

Continued

REAGENT or RESOURCE	SOURCE	IDENTIFIER
5-(1-(4-(*tert*-Butyl)phenyl)-1*H*-1,2,3-triazol-4-yl)-3-methoxy-1*H*-pyrrole-2-carbaldehyde (**A2**)	This Manuscript	
2-Azidoethan-1-ol (**B1**)	This Manuscript (see also ref.[37])	
5-(1-(2-Hydroxyethyl)-1*H*-1,2,3-triazol-4-yl)-3-methoxy-1*H*-pyrrole-2-carbaldehyde (**B2**)	This Manuscript	
N-((*E*)-(5-(1-(4-(*tert*-Butyl)phenyl)-1*H*-1,2,3-triazol-4-yl)-3-methoxy-1*H*-pyrrol-2-yl)methylene)adamantan-1-aminium chloride (**1**)	This Manuscript	
(*E*)-*N*-((5-(1-(4-(*tert*-Butyl)phenyl)-1*H*-1,2,3-triazol-4-yl)-3-methoxy-1*H*-pyrrol-2-yl)methylene)cyclopentanaminium chloride (**2**)	This Manuscript	
(*E*)-*N*-((5-(1-(4-(*tert*-Butyl)phenyl)-1*H*-1,2,3-triazol-4-yl)-3-methoxy-1*H*-pyrrol-2-yl)methylene)-2-hydroxyethan-1-aminium chloride (**3**)	This Manuscript	
(*E*)-2-Hydroxy-*N*-((5-(1-(2-hydroxyethyl)-1*H*-1,2,3-triazol-4-yl)-3-methoxy-1*H*-pyrrol-2-yl)methylene)ethan-1-aminium chloride (**4**)	This Manuscript	
N-((*E*)-(5-(1-(2-Hydroxyethyl)-1*H*-1,2,3-triazol-4-yl)-3-methoxy-1*H*-pyrrol-2-yl)methylene)adamantan-1-aminium chloride (**5**)	This Manuscript	
(*E*)-*N*-((5-(1-(4-Chlorophenyl)-1*H*-1,2,3-triazol-4-yl)-3-methoxy-1*H*-pyrrol-2-yl)methylene)cyclohexanaminium chloride (**6**)	Faculty of Sciences, University of Burgos (see also ref.[26])	
Critical commercial assays		
Lactate-Glo™ Assay Kit	Promega	J5022
Pierce™ BCA Protein Assay Kit	Thermo Fisher Scientific	23227
Deposited data		
Structure of compound **6**·Lac	This Manuscript; Cambridge Crystallographic Data Centre	CCDC: 2258886
Experimental models: Cell lines		
Human: CAL27 cells	ATCC	CRL-2095
Human: HeLa cells	ATCC	CCL-2
Human: MCF7 cells	ATCC	HTB-22
Human: MCF10A cells	ATCC	CRL-10317
Software and algorithms		
ALOGPS 2.1	VCCLAB website	https://vcclab.org/lab/alogps
BindFit v0.5	BindFit website	http://app.supramolecular.org/bindfit
ChemDraw Professional 20	PerkinElmer	https://perkinelminformatics.com
Compusyn v1.0	Combosyn	https://www.combosyn.com
MestReNova	Mestrelab	https://mestrelab.com
Olex2	OlexSys Ltd	https://www.olexsys.org/olex2
OriginPro 8.6	OriginLab®	https://www.originlab.com
Prism v8.0.1	Graph-Pad	https://www.graphpad.com/features
SHELXL-2016	SHELX website	https://shelx.uni-goettingen.de
SHELXT	SHELX website	https://shelx.uni-goettingen.de

RESOURCE AVAILABILITY

Lead contact

Further information and requests for resources should be directed to and will be fulfilled by the lead contact, Roberto Quesada (rquesada@ubu.es).

Materials availability

All materials generated in this study are available from the lead contact without restriction.

Data and code availability

- Experimental details, NMR, HR-MS, absorption and emission spectra and characterisation data of the synthesised compounds, and results of NMR titration and transmembrane anion transport experiments are available in the STAR Methods and in the supplemental information.
- The supplemental crystallographic data for compound **6**·Lac have been deposited at the Cambridge Crystallographic Data Centre (12 Union Road, Cambridge CB2 1EZ, UK) under accession number CCDC 2258886. These data can be obtained free of charge from https://www.ccdc.cam.ac.uk/structures/.
- Any additional information required to reanalyse the data reported in this paper is available from the lead contact upon request.

EXPERIMENTAL MODEL AND STUDY PARTICIPANT DETAILS

Cellular models

Human cell lines HeLa (cervix adenocarcinoma isolated from a female patient), CAL27 (oral squamous cell carcinoma isolated from a male patient), MCF7 (breast adenocarcinoma isolated from a female patient) and MCF10A (non-cancer epithelial breast cells isolated from a female patient) were obtained from the American Type Culture Collection (ATCC, Manassas, VA, USA). These cell lines were tested and verified by ATCC using short tandem repeat analysis. They were cultured between passage number 10−30 and were routinely tested for mycoplasma contamination detection. HeLa and CAL27 cells were cultured in Dulbecco's Modified Eagle's Medium (DMEM, Biological Industries, Beit Haemek, Israel) supplemented with 10% heat-inactivated fetal bovine serum (FBS), 100 U/mL penicillin, 100 μg/mL streptomycin, and 2 mM glutamine. MCF7 cells were cultured in DMEM/F12 medium supplemented with 10% heat-inactivated FBS, 100 U/mL penicillin, 100 μg/mL streptomycin, 2 mM glutamine, 50 μM sodium pyruvate, and 10 μg/mL insulin. MCF10A cells were cultured in DMEM/F12 medium supplemented with 5% horse serum, 100 U/mL penicillin, 100 μg/mL streptomycin, 2 mM glutamine, 0.5 μg/mL hydrocortisone, 20 ng/mL EGF, 100 ng/mL choleric toxin, and 10 μg/mL insulin. In experiments where lactate concentrations were determined, standard FBS was replaced by dialysed FBS (lactate free). All cell lines were grown at 37°C in an incubator with 5% CO_2 atmosphere.

In reference to the cell lines employed in our study, it is noteworthy that the HeLa cell line holds substantial recognition as one of the most extensively investigated cell lines in cancer research, if not the most extensively studied. It is characterized by a heightened glycolytic rate, which aligns with our research objectives. Similarly, the MCF7 cell line is widely explored in the realm of cancer research and serves as an exceptional model for understanding breast cancer, which bears significant global implications. Conversely, the MCF10A cell line represents a non-malignant mammary cell type, allowing us to establish a comparative foundation for discerning divergences between cancerous and non-cancerous characteristics. Finally, CAL27 cells exhibit a distinct genetic background compared to the previously mentioned cell lines. This variation in genetic composition adds further diversity to our study and enables us to investigate the impact of different genetic backgrounds on our experimental findings.

METHOD DETAILS

Synthesis and characterisation of compounds

Commercial reagents were employed as received without any further purification. ^{1}H, ^{13}C(^{1}H) and DEPT-135 NMR spectra were recorded at 298 K on a Varian Mercury-300 MHz spectrometer, employing $CDCl_3$ or DMSO-d_6 as solvents, with their residual signals being used to reference the spectra; DEPT-135 experiments were conducted to assign carbon-13 signals. Chemical shifts are reported in parts per million with respect to residual solvent protons and coupling constants in hertz. High-resolution mass spectra were recorded on an Agilent 6545 Q-TOF mass spectrometer coupled to a 1260 Infinity liquid chromatographer from the same brand; the ionisation source employed was electrospray in its positive mode. Absorption and emission spectra were recorded on Hitachi U-3900 and F-7000 spectrophotometers, respectively. X-ray diffraction studies were carried out at 100 K on a Bruker D8 VENTURE diffractometer.

Synthesis of 1-azido-4-(tert-butyl)benzene (A1)
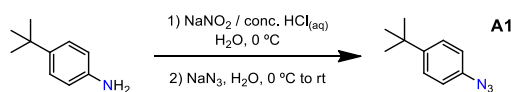
4-(*tert*-Butyl)aniline (2.1 mL, 13.0 mmol) was mixed with a concentrated HCl aqueous solution (20 mL) and the obtained mixture was stirred vigorously at 0°C (ice bath) for 15 min. The aniline was not dissolved. A solution of sodium nitrite (1.37 g, 19.9 mmol, 1.5 equiv.) in water (15 mL) was added in a dropwise manner over a period of 5 min; formation of a yellow solution was observed. The mixture was stirred at 0°C for an additional 30 min. A solution of sodium azide (1.74 g, 26.8 mmol, 2.1 equiv.) in water (15 mL) was added dropwise at 0°C within 5 min and the resulting reaction mixture was stirred vigorously at room temperature for a further 3 h; addition of the sodium azide solution resulted in the disappearance of the yellow colour. The mixture was extracted with ethyl acetate (3 × 35 mL), the extracts were combined, washed with water (1 × 50 mL), dried over anhydrous sodium sulfate, filtered and concentrated under reduced pressure to give compound **A1** as a yellow liquid (1.7 g, 74%).

^{1}H-NMR (300 MHz, CDCl$_3$): δ 7.43-7.35 (m, 2H), 7.02-6.95 (m, 2H), 1.33 (s, 9H). ^{13}C(^{1}H)-NMR (75 MHz, CDCl$_3$): δ 148.1 (ArC), 137.2 (ArC), 126.8 (ArCH), 118.7 (ArCH), 34.6 (C), 31.5 (CH$_3$). HR-MS (ESI$^+$): No satisfactory HR-MS (ESI$^+$) analysis result was obtained for this compound.

Synthesis of 5-(1-(4-(tert-butyl)phenyl)-1H-1,2,3-triazol-4-yl)-3-methoxy-1H-pyrrole-2-carbaldehyde (A2)
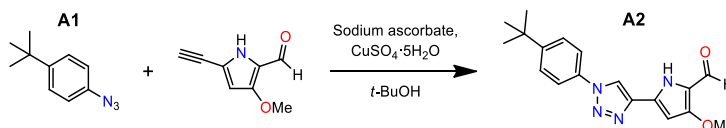
5-ethynyl-3-methoxy-1H-pyrrole-2-carbaldehyde, synthesised as reported in the literature[36] (1.47 g, 9.86 mmol), and compound **A1** (1.71 g, 9.76 mmol) were dissolved partially in *tert*-butanol (20 mL) in a 250-mL Schlenk tube. A solution of (+)-sodium L-ascorbate (389 mg, 1.96 mmol, 0.2 equiv.) in water (10 mL) and a solution of CuSO$_4$·5H$_2$O (243 mg, 0.97 mmol, 0.1 equiv.) in water (10 mL) were subsequently added to the resulting suspension. A gradual change of colour from dark brown to pale brown was observed upon addition of the CuSO$_4$ solution. The tube was closed with a stopper and the reaction mixture was stirred at room temperature for 18 h. The content of the flask was poured into water (100 mL) and the precipitate was filtered out and washed with water (3 × 30 mL) and diethyl ether (1 × 30 mL). NMR analysis revealed that compound **A2** was still contaminated with compound **A1**, so diethyl ether (roughly 50 mL) was added to the product and the resulting suspension stirred at room temperature for 15 min. The solid was filtered out and air-dried to give compound **A2**, now pure, as a brown non-crystalline solid (1.96 g, 62%).

^{1}H-NMR (300 MHz, DMSO-d_6): δ 12.08 (s, 1H), 9.47 (s, 1H), 9.09 (s, 1H), 7.77 (d, J = 8.7 Hz, 2H), 7.66 (d, J = 8.7 Hz, 2H), 6.53 (d, J = 2.4 Hz, 1H), 3.90 (s, 3H), 1.34 (s, 9H). ^{13}C(^{1}H)-NMR (75 MHz, DMSO-d_6): δ 173.9 (CHO), 157.8 (ArC), 151.8 (ArC), 140.2 (ArC), 134.0 (ArC), 129.4 (ArC), 126.9 (ArCH), 120.1 (ArCH), 119.9 (ArCH), 118.7 (ArC), 93.7 (ArCH), 58.1 (CH$_3$), 34.6 (C), 31.0 (CH$_3$). HR-MS (ESI$^+$) *m/z*: [M+H]$^+$ calcd. 325.1665, found 325.1644.

Synthesis of 2-azidoethan-1-ol (B1)
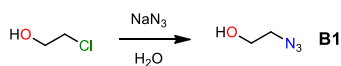
The procedure to prepare this compound was adapted from the literature.[37] A solution of sodium azide (2 g, 30.8 mmol) in water (8.8 mL) was added dropwise to a solution of 2-chloroethanol (416 µL, 6.21 mmol) in water (6.2 mL) over a period of 30 minutes. The reaction mixture was stirred and heated to reflux for 22 h. Upon cooling to room temperature, this solution was extracted with ethyl acetate (3 x 30 mL), and the organic phase was dried over anhydrous sodium sulfate, filtered and concentrated to dryness to give compound **B1** as a yellow oil (384 mg, 71%).

^{1}H-NMR (300 MHz, CDCl$_3$): δ 3.98 (s, 1H), 3.63-3.59 (m, 2H), 3.28-3.24 (m, 2H). ^{13}C(^{1}H)-NMR (75 MHz, CDCl$_3$): δ 60.8 (CH$_2$), 52.9 (CH$_2$). HR-MS (ESI$^+$): no satisfactory HR-MS analysis was obtained for this compound.

Synthesis of 5-(1-(2-hydroxyethyl)-1H-1,2,3-triazol-4-yl)-3-methoxy-1H-pyrrole-2-carbaldehyde (B2)
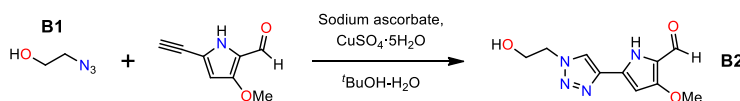
5-ethynyl-3-methoxy-1H-pyrrole-2-carbaldehyde, synthesised as reported in the literature[36] (524 mg, 3.51 mmol), and azide **B1** (384 mg, 4.41 mmol, 1.25 equiv.) were dissolved partially in *tert*-butanol (16 mL). A solution of (+)-sodium L-ascorbate (140 mg, 0.71 mmol, 0.20 equiv.) in water (8 mL) and a solution of CuSO$_4$·5H$_2$O (100 mg, 0.40 mmol, 0.11 equiv.) in water (8 mL) were successively added to the suspension. The reaction mixture was stirred at room temperature for 24 h and *tert*-butanol removed under reduced pressure. The brown solid, compound **B2**, was isolated by vacuum filtration, washed with water (10 mL) and diethyl ether (10 mL) and dried *in vacuo* (695 mg, 84%).

^{1}H-NMR (300 MHz, DMSO-d_6): δ 11.99 (s, 1H), 9.43 (s, 1H), 8.55 (s, 1H), 6.45 (s, 1H), 5.04-5.18 (m, 1H), 4.54-4.38 (m, 2H), 3.87 (s, 3H), 3.83-3.71 (m, 2H). ^{13}C(^{1}H)-NMR (75 MHz, DMSO-d_6): δ 173.7 (CHO), 158.1 (ArC), 139.3 (ArC), 130.5 (ArC), 122.7 (ArCH), 118.6 (ArC), 93.3 (ArCH), 59.9 (CH$_2$), 58.1 (CH$_3$), 52.6 (CH$_2$). HR-MS (ESI$^+$) *m/z*: [M+H]$^+$ calcd. 237.0982, found 237.0991.

Synthesis of N-((E)-(5-(1-(4-(tert-butyl)phenyl)-1H-1,2,3-triazol-4-yl)-3-methoxy-1H-pyrrol-2-yl)methylene)adamantan-1-aminium chloride (1)
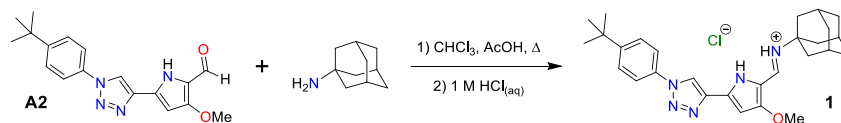
A mixture of aldehyde **A2** (120 mg, 0.37 mmol), 1-adamantylamine (112 mg, 0.74 mmol, 2.0 equiv.) and glacial acetic acid (100 μL) in chloroform (15 mL) was stirred at 65°C for 72 h. Upon cooling to room temperature the chloroform was evaporated under reduced pressure and the residue redissolved in dichloromethane (25 mL). The solution of the crude compound was washed with a 1 M HCl aqueous solution (3 × 25 mL); the organic phase was dried over anhydrous sodium sulfate, filtered and evaporated to dryness under reduced pressure. The residue was recrystallised from a mixture of dichloromethane and *n*-hexane to give compound **1** as a brown solid (116 mg, 64%).

^{1}H-NMR (300 MHz, CDCl$_3$): δ 13.76 (s, 1H), 11.24 (d, J = 15.4 Hz, 1H), 9.08 (s, 1H), 7.73 (d, J = 8.4 Hz, 2H), 7.66 (d, J = 15.9 Hz, 1H), 7.53 (d, J = 8.4 Hz, 2H), 6.54 (s, 1H), 3.95 (s, 3H), 2.21 (s$_b$, 3H), 2.12-1.91 (m, 6H), 1.76-1.66 (m, 6H), 1.34 (s, 9H). ^{13}C(^{1}H)-NMR (75 MHz, CDCl$_3$): δ 162.9 (ArC), 152.7 (ArC), 139.7 (ArC), 139.1 (CH), 138.6 (ArC), 134.1 (ArC), 126.8 (ArCH), 121.3 (ArCH), 120.6 (ArCH), 111.4 (ArC), 93.5 (ArCH), 58.7 (CH$_3$), 57.4 (C), 42.2 (CH$_2$), 35.6 (CH$_2$), 34.9 (C), 31.3 (CH$_3$), 29.3 (CH). **HR-MS** (ESI$^+$) *m/z*: [M+H]$^+$ calcd. 458.2914, found 458.2920.

Synthesis of (E)-N-((5-(1-(4-(tert-butyl)phenyl)-1H-1,2,3-triazol-4-yl)-3-methoxy-1H-pyrrol-2-yl)methylene)cyclopentanaminium chloride (2)
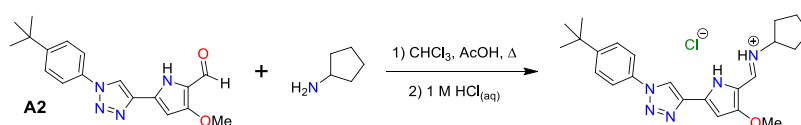
A mixture of aldehyde **A2** (104 mg, 0.32 mmol), cyclopentylamine (95 μL, 0.93 mmol, 3.0 equiv.) and glacial acetic acid (100 μL) in chloroform (15 mL) was stirred at 65°C for 14 h. Upon cooling to room temperature the chloroform was evaporated under reduced pressure and the residue redissolved in dichloromethane (15 mL). The solution of the crude compound was washed with a 1 M HCl aqueous solution (3 × 15 mL); the organic phase was dried over anhydrous sodium sulfate, filtered and evaporated to dryness under reduced pressure. The residue was recrystallised from a mixture of dichloromethane and *n*-hexane to give compound **2** as a brown solid (86 mg, 66%).

^{1}H-NMR (300 MHz, CDCl$_3$): δ 13.81 (s, 1H), 11.37-11.11 (m, 1H), 9.07 (s, 1H), 7.73 (d, J = 8.7 Hz, 2H), 7.65 (d, J = 15.4 Hz, 1H), 7.54 (d, J = 8.7 Hz, 2H), 6.55 (d, J = 2.1 Hz, 1H), 4.05-3.90 (s+m, 4H), 2.13-1.89 (m, 6H), 1.76-1.60 (m, 2H), 1.36 (s, 9H). ^{13}C(^{1}H)-NMR (75 MHz, CDCl$_3$): δ 163.1 (ArC), 152.7 (ArC), 142.6 (CH), 139.6 (ArC), 138.8 (ArC), 134.0 (ArC), 126.8 (ArCH), 121.3 (ArCH), 120.5 (ArCH), 111.3 (ArC), 93.5 (ArCH), 63.3 (CH), 58.7 (CH$_3$), 34.9 (C), 33.4 (CH$_2$), 31.3 (CH$_3$), 23.8 (CH$_2$). **HR-MS** (ESI$^+$) *m/z*: [M+H]$^+$ calcd. 392.2445, found 392.2452.

*Synthesis of (E)-N-((5-(1-(4-(tert-butyl)phenyl)-1H-1,2,3-triazol-4-yl)-3-methoxy-1H-pyrrol-2-yl)methylene)-2-hydroxyethan-1-aminium chloride (3)*
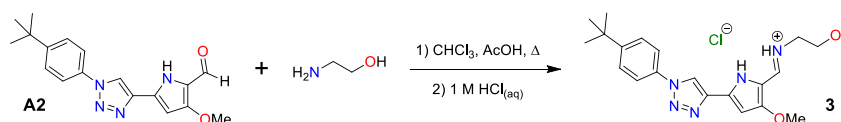
A mixture of aldehyde **A2** (100 mg, 0.31 mmol), ethanolamine (92 μL, 1.52 mmol, 5.0 equiv.) and glacial acetic acid (100 μL) in chloroform (15 mL) was stirred at 65°C for 20 h. Upon cooling to room temperature the chloroform was evaporated under reduced pressure and the residue redissolved in a mixture of dichloromethane (15 mL) and methanol (5 mL). The solution of the crude compound was washed with a 1 M HCl aqueous solution (3 × 25 mL). The combined aqueous phase was extracted with dichloromethane several times and, after putting together the different organic phases, the combined one was dried over anhydrous sodium sulfate, filtered and evaporated to dryness under reduced pressure. The residue was recrystallised from a mixture of dichloromethane and *n*-hexane to give compound **3** as a brown solid (95 mg, 76%).

^{1}H-NMR (300 MHz, CDCl$_3$): δ 13.26 (s, 1H), 10.91-10.86 (m, 1H), 8.92 (s, 1H), 7.74 (d, J = 8.5 Hz, 2H), 7.66 (d, J = 15.1 Hz, 1H), 7.55 (d, J = 8.5 Hz, 2H), 6.41 (s, 1H), 4.06 (s$_b$, 1H), 3.97 (s$_b$, 2H), 3.80 (s, 3H), 3.75-3.64 (m, 2H), 1.36 (s, 9H). ^{13}C(^{1}H)-NMR (75 MHz, CDCl$_3$): δ 163.6 (ArC), 152.9 (ArC), 145.2 (CH), 139.4 (ArC), 139.3 (ArC), 134.0 (ArC), 126.9 (ArCH), 121.1 (ArCH), 120.4 (ArCH), 111.6 (ArC), 93.7 (ArCH), 60.4 (CH$_2$), 58.7 (CH$_3$), 53.5 (CH$_2$), 35.0 (C), 31.4 (CH$_3$). **HR-MS** (ESI$^+$) *m/z*: [M+H]$^+$ calcd. 368.2081, found 368.2086.

Synthesis of (E)-2-hydroxy-N-((5-(1-(2-hydroxyethyl)-1H-1,2,3-triazol-4-yl)-3-methoxy-1H-pyrrol-2-yl)methylene)ethan-1-aminium chloride (4)
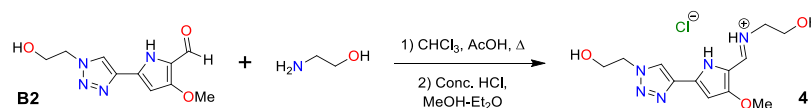
A mixture of aldehyde **B2** (102 mg, 0.43 mmol), ethanolamine (31 μL, 0.52 mmol, 1.20 equiv.) and glacial acetic acid (100 μL) in chloroform (15 mL) was stirred at 65°C for 16 h. Upon cooling to room temperature the chloroform was evaporated under reduced pressure and the residue suspended in a mixture of diethyl ether (12 mL) and methanol (3 mL); concentrated hydrochloric acid (120 μL) was added and the mixture stirred at room temperature for 16 h. The resulting brown solid, compound **4**, was isolated by vacuum filtration, washed with dichloromethane (5 mL) and diethyl ether (5 mL), and dried _in vacuo_ (62 mg, 46%).

^{1}H-NMR (300 MHz, DMSO-d_6): δ 13.00 (s, 1H), 10.96-10.90 (m, 1H), 8.68 (s, 1H), 8.18 (d, J = 14.8 Hz, 1H), 6.68-6.62 (m, 1H), 5.15 (s$_b$, 2H), 4.54-4.51 (m, 2H), 3.97 (s, 3H), 3.83-3.80 (m, 2H), 3.69-3.62 (m, 4H). [13]C(^{1}H)-NMR (75 MHz, DMSO-d_6): δ 162.8 (ArC), 146.9 (CH), 137.9 (ArC), 137.5 (ArC), 124.6 (ArCH), 110.1 (ArC), 94.0 (ArCH), 59.7 (CH$_2$), 59.5 (CH$_2$), 58.8 (CH$_3$), 52.8 (CH$_2$), 52.4 (CH$_2$). **HR-MS** (ESI[+]) _m/z_: [M+H][+] calcd. 280.1404, found 280.1413.

Synthesis of N-((E)-(5-(1-(2-Hydroxyethyl)-1H-1,2,3-triazol-4-yl)-3-methoxy-1H-pyrrol-2-yl)methylene)adamantan-1-aminium chloride (5)
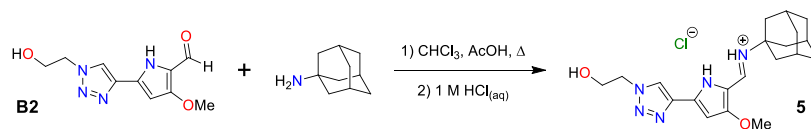
A mixture of aldehyde **B2** (102 mg, 0.43 mmol), 1-adamantylamine (78 mg, 0.52 mmol, 1.20 equiv.) and glacial acetic acid (100 μL) in chloroform (15 mL) was stirred at 65°C for 20 h. Upon cooling to room temperature the chloroform was evaporated under reduced pressure and the residue redissolved in dichloromethane (20 mL). The solution of the crude compound was washed with a 1 M HCl aqueous solution (3 × 30 mL); the organic phase was dried over anhydrous sodium sulfate, filtered and evaporated to dryness under reduced pressure. The residue was recrystallised from a mixture of dichloromethane and _n_-hexane to give compound **5** as a brown solid (106 mg, 61%).

^{1}H-NMR (300 MHz, DMSO-d_6): δ 13.38 (s, 1H), 11.36 (d, J = 15.8 Hz, 1H), 8.66 (s, 1H), 7.95 (d, J = 15.8 Hz, 1H), 6.64 (s, 1H), 5.18 (s, 1H), 4.61-4.45 (m, 2H), 3.97 (s, 3H), 3.86-3.74 (m, 2H), 2.14 (s, 3H), 1.96 (s, 6H), 1.66 (s, 6H). [13]C(^{1}H)-NMR (75 MHz, DMSO-d_6): δ 162.6 (ArC), 140.7 (CH), 137.9 (ArC), 137.5 (ArC), 124.4 (ArCH), 110.3 (ArC), 93.9 (ArCH), 59.7 (CH$_2$), 58.8 (CH$_3$), 56.6 (C), 52.8 (CH$_2$), 41.0 (CH$_2$), 35.0 (CH$_2$), 28.7 (CH). **HR-MS** (ESI[+]) _m/z_: [M+H][+] calcd. 370.2238, found 370.2256.

X-ray diffraction studies

Single crystals of the **6**·Lac complex were obtained by slow evaporation of a 2:1 MeOH/_n_-BuOH solution containing 1 equiv. of compound **6** and 2 equiv. of sodium L-lactate.

Three dimensional X-ray data were collected on a Bruker D8 VENTURE diffractometer. Data were corrected for absorption effects using the multi-scan method (SADABS).[38] Complex scattering factors were taken from the SHELXL-2016 programme[39] running under the Olex2 programme.[40] The structure was solved with SHELXT[41] and refined as a two-component inversion twin by full-matrix least-squares on F[2]. All hydrogen atoms were included in calculated positions and refined in riding mode, except those linked to O(5) and O(10), that were refined freely. Refinement converged with anisotropic displacement parameters for all non-hydrogen atoms. Crystal data and details on data collection and refinement are summarised in Table S1. The structure was drawn with the Olex2 programme.[40]

^{1}H-NMR binding studies

Chloride complexes

Generally, 800 μL of a 50 mM solution of the corresponding compound in DMSO-d_6 were prepared and the ^{1}H NMR spectrum of this solution was recorded. Aliquots of this solution were taken to prepare 35 and 25 mM solutions of the compound, which spectra were recorded. From the former 17.5, 8.75, 4.38, 2.19, 1.09 and 0.55 mM solutions were prepared, while from the latter 12.5, 6.25, 3.13, 1.56, 0.78 and 0.39 mM solutions were prepared, and their spectra were recorded. Due to solubility issues, a 50 mM solution could not be prepared for compound **1**; the first spectrum corresponds to a 10.3 mM solution. From this solution the following ones were prepared: 8.99, 6.42, 4.50, 3.21, 2.25, 1.61, 1.12, 0.80, 0.56 and 0.40 mM. All spectra were registered at 298 K.

For each ^{1}H NMR stack plot, the signals of the protons of the imine and pyrrole NH groups and of the triazole CH group of the molecules were monitored for changes in chemical shift, which provided several data sets that were employed in the determination of association

constants K_a. Fitting was performed with the Bindfit software.[29,30] In all cases data were fitted satisfactorily to the 1:1 (LH:Cl) binding model, LH being the protonated receptor and Cl the chloride anion. In some cases the last spectra recorded, although included in the stack plot, were not considered for fitting, since the signals (especially those corresponding to the NH protons) are too broad to identify their shifts unequivocally.

Titration of compound 6 with NaLac and TBAOH

2 mL of a DMSO-d_6 stock solution of compound **6** (host) were prepared (0.01 M). From this solution, 1 mL was taken to prepare the solution of the titrating agent (guest; sodium L-lactate or tetrabutylammonium hydroxide); in this way the dilution effect is avoided. 0.5 mL of the solution of the host were put into an NMR tube, which was capped with a septum, and the ^{1}H NMR spectrum was recorded. Subsequently, an aliquot of the solution of the guest was added with a proper microsyringe through the septum, the solution homogenised and the spectrum recorded. This process was repeated 18 times.

Transmembrane anion transport experiments

Preparation of phospholipid vesicles

A chloroform solution of 1-palmitoyl-2-oleoyl-*sn*-glycero-3-phosphocoline (POPC) (20 mg/mL) (Sigma-Aldrich) (or a 7:3 POPC:cholesterol mixture, in the case of HPTS- and lucigenin-based assays) was evaporated *in vacuo* using a rotary evaporator and the resulting film was dried under high vacuum for, at least, 2 h. Different aqueous solutions were used to rehydrate the lipid film: (a) ISE assays: 489 mM NaCl, 5 mM NaH$_2$PO$_4$, I.S. 500 mM, pH 7.2, for Cl$^-$/NO$_3^-$ exchange experiments, or 451 mM NaCl, 20 mM NaH$_2$PO$_4$, I.S. 500 mM, pH 7.2, for Cl$^-$/HCO$_3^-$ or Cl$^-$/Lac$^-$ exchange experiments, as well as Cl$^-$/SO$_4^{2-}$ assays; (b) carboxyfluorescein (CF)-based assays: 451 mM NaCl, 20 mM NaH$_2$PO$_4$, 50 mM CF, I.S. 500 mM, pH 7.2; (c) HPTS-based assays: 126.2 mM NaNO$_3$, 10 mM NaH$_2$PO$_4$, 1 mM HPTS, I.S. 150 mM, pH 6.2; (d) lucigenin-based assays: 102.2 mM NaNO$_3$, 20 mM NaH$_2$PO$_4$, 1 mM lucigenin, I.S. 150 mM, pH 7.2. The resulting suspension was vortexed and subjected to nine freeze-thaw cycles; subsequently, it was extruded twenty-nine times through a polycarbonate membrane (200 nm) employing a LiposoFast basic extruder (Avestin, Inc.). The resulting unilamellar vesicles were: (a) ISE assays: dialysed against a NaNO$_3$ aqueous solution (489 mM NaNO$_3$, 5 mM NaH$_2$PO$_4$, I.S. 500 mM, pH 7.2, for Cl$^-$/NO$_3^-$ exchange experiments) or a Na$_2$SO$_4$ aqueous solution (150 mM Na$_2$SO$_4$, 20 mM NaH$_2$PO$_4$, I.S. 500 mM, pH 7.2, for Cl$^-$/HCO$_3^-$ or Cl$^-$/Lac$^-$ exchange assays, as well as Cl$^-$/SO$_4^{2-}$ experiments) to remove unencapsulated chloride; (b) carboxyfluorescein-based assays: subjected to size-exclusion chromatography, using Sephadex® G-25 as the stationary phase and a Na$_2$SO$_4$ aqueous solution (150 mM Na$_2$SO$_4$, 20 mM NaH$_2$PO$_4$, I.S. 500 mM, pH 7.2) as the mobile phase, to remove unencapsulated carboxyfluorescein; (c) HPTS-based assays: subjected to size-exclusion chromatography, using Sephadex® G-25 as the stationary phase and the inner solution without HPTS (126.2 mM NaNO$_3$, 10 mM NaH$_2$PO$_4$, I.S. 150 mM, pH 6.2) as the mobile phase, to remove unencapsulated HPTS; (d) lucigenin-based assays: subjected to size-exclusion chromatography, using Sephadex® G-25 as the stationary phase and the inner solution without lucigenin (102.2 mM NaNO$_3$, 20 mM NaH$_2$PO$_4$, I.S. 150 mM, pH 7.2) as the mobile phase, to remove unencapsulated lucigenin. Vesicles were collected in a 10-mL volumetric flask, using either the external solution (ISE and carboxyfluorescein-based assays) or the inner one without the probe (HPTS- and lucigenin-based assays) to bring the suspension to the desired volume.

In the case of ^{13}C NMR experiments, 6 mL of the above-mentioned chloroform solution of POPC (20 mg/mL) (Sigma-Aldrich) were evaporated to dryness using a rotary evaporator and the resulting film was dried under high vacuum for, at least, 2 h. The lipid film was rehydrated by addition of 2 mL of a CH$_3$CH(OH)^{13}CO$_2$Na aqueous solution (200 mM NaLac, 20 mM NaH$_2$PO$_4$, pH 7.2), prepared with an aqueous solution of isotopically labelled sodium L-lactate [45-55% (w/w)] (Sigma-Aldrich). The suspension was vortexed and subjected to nine freeze-thaw cycles, followed by its extrusion (29 times) through a polycarbonate membrane (200 nm) using a LiposoFast basic extruder (Avestin, Inc.). The resulting unilamellar vesicles were dialysed against a Na$_2$SO$_4$ buffered aqueous solution (150 mM Na$_2$SO$_4$, 20 mM NaH$_2$PO$_4$, pH 7.2) to remove unencapsulated L-lactate. This suspension was used as such.

ISE-based assays

Unilamellar vesicles (mean diameter: 200 nm) made of POPC and containing a NaCl aqueous solution (489 mM NaCl, 5 mM NaH$_2$PO$_4$, I.S. 500 mM, pH 7.2, for Cl$^-$/NO$_3^-$ exchange experiments, or 451 mM NaCl, 20 mM NaH$_2$PO$_4$, I.S. 500 mM, pH 7.2, for Cl$^-$/HCO$_3^-$ or Cl$^-$/Lac$^-$ exchange experiments, as well as Cl$^-$/SO$_4^{2-}$ assays) were dispersed in a NaNO$_3$ aqueous solution (489 mM NaNO$_3$, 5 mM NaH$_2$PO$_4$, I.S. 500 mM, pH 7.2, for Cl$^-$/NO$_3^-$ exchange experiments) or a Na$_2$SO$_4$ aqueous solution (150 mM Na$_2$SO$_4$, 20 mM NaH$_2$PO$_4$, I.S. 500 mM, pH 7.2, for Cl$^-$/HCO$_3^-$ or Cl$^-$/Lac$^-$ exchange experiments, as well as Cl$^-$/SO$_4^{2-}$ assays), the final lipid concentration during the assays being 0.5 mM and the final volume 5 mL. In the case of Cl$^-$/NO$_3^-$ exchange experiments and Cl$^-$/SO$_4^{2-}$ assays, a certain volume of a solution of the corresponding compound in DMSO (or the blank, DMSO, 12.5 μL) was added at t = 0 s, and the chloride released was monitored for 300 s with a chloride-selective electrode (Fisherbrand™ accumet™ chloride combination electrode, Cat. No. 13-620-627). At t = 300 s a surfactant (Triton-X, 20% dispersion in water, 20 μL) was added to lyse vesicles and free all encapsulated chloride. This value was considered as 100% release. Regarding Cl$^-$/HCO$_3^-$ and Cl$^-$/Lac$^-$ exchange assays, a 500 mM NaHCO$_3$ or NaLac aqueous solution prepared with the Na$_2$SO$_4$ one (150 mM Na$_2$SO$_4$, 20 mM NaH$_2$PO$_4$, I.S. 500 mM, pH 7.2) was added at t = -10 s to the vesicles suspension, the HCO$_3^-$ or Lac$^-$ concentration during the assay being 40 mM. The rest of the experimental procedure is similar to that described previously. EC$_{50}$ and Hill parameter values (*n*) are presented in Table S2.

^{13}C NMR-based assays

Vesicles made of POPC were loaded with a $CH_3CH(OH)^{13}CO_2Na$ aqueous solution (200 mM NaLac, 20 mM NaH_2PO_4, pH 7.2) and treated according to the procedure described previously. 380 μL of this suspension were placed in an NMR tube, and 40 μL of D_2O and 3 μL of DMSO were added. This suspension was vortexed and a ^{13}C NMR spectrum recorded (80 pulses). Then, a NaCl aqueous solution was added in such a way that the external chloride concentration during the experiment was 50 mM. This was followed by the addition of a DMSO solution of the corresponding compound (**1** or **3**), its concentration in the suspension being 1% mol in both cases. The suspension was vortexed and a ^{13}C NMR spectrum recorded again (80 pulses). Finally, a $MnCl_2$ aqueous solution was added in such a way that the Mn^{2+} concentration during the assay was 0.5 mM, and a ^{13}C NMR spectrum was acquired (80 pulses).

Carboxyfluorescein-based assays

Vesicles made of POPC were loaded with a NaCl aqueous solution (451 mM NaCl, 20 mM NaH_2PO_4, 50 mM CF, I.S. 500 mM, pH 7.2) and treated according to the procedure described previously. Experiments were performed in 1-cm disposable cells, the final POPC concentration in the cuvette being 0.05 mM and the total volume 2.5 mL. At t = 60 s an aliquot of a solution of the corresponding compound in DMSO (or the blank, DMSO, 1.25 μL) was added, and emission changes were recorded for 300 s. At t = 360 s a pulse of a detergent (Triton™ X-100, 20% dispersion in water, 20 μL) was added to lyse vesicles and free all entrapped CF. The obtained emission value was regarded as 100% release and used to normalise data. Data for compound **6** were taken from ref.[26]

HPTS-based assays

First of all, a calibration curve matching I_{460}/I_{403}, the relationship between the emission intensity at 460 nm and that at 403 nm (corresponding to the excitation wavelengths of the dye's deprotonated and protonated forms, respectively) of an HPTS aqueous solution (15 nM), prepared with a $NaNO_3$ aqueous solution (126.2 mM $NaNO_3$, 10 mM NaH_2PO_4), and pH was built. In order to do it, aliquots of a NaOH aqueous solution (0.5 M), prepared with a $NaNO_3$ aqueous solution (126.2 mM $NaNO_3$, 10 mM NaH_2PO_4), were successively added to the HPTS solution, and after each addition the ratio of emission intensities at 460 and 403 nm and the pH value of the solution were recorded. Data were fitted to an *S*-logistic model, which provided an R^2 = 0.9999 (Figure S82).

7:3 POPC:cholesterol vesicles were loaded with a $NaNO_3$ aqueous solution (126.2 mM $NaNO_3$, 10 mM NaH_2PO_4, 1 mM HPTS, I.S. 150 mM, pH 6.2) and treated according to the procedure described previously. Experiments were performed in 1-cm disposable cells, the final POPC concentration in the cuvette being 0.5 mM and the final volume 2.5 mL. Just before starting the measurements the required volume of the vesicles stock solution was suspended in the outer solution (126.2 mM $NaNO_3$, 10 mM NaH_2PO_4, I.S. 150 mM, pH 7.5). At t = 60 s an aliquot of a solution of the corresponding compound in DMSO (or the blank, DMSO, 6.25 μL) was added, and the ratio of emission intensities at 460 and 403 nm was recorded for five more minutes. At t = 360 s a detergent (Triton™ X-100, 20% dispersion in water, 20 μL) was added, to lyse vesicles and balance pH.

Lucigenin-based assays

Firstly, the ability of L-lactate to quench lucigenin's fluorescence was examined. Aliquots of a buffered aqueous solution of NaLac (100 mM NaLac, 30 μM lucigenin, 102.2 mM $NaNO_3$, 20 mM NaH_2PO_4, pH 7.2) were successively added to a buffered aqueous solution of lucigenin (30 μM lucigenin, 102.2 mM $NaNO_3$, 20 mM NaH_2PO_4, pH 7.2), and the emission spectrum obtained after each addition was recorded (excitation wavelength: 372 nm) (Figure S89).

The quenching of the fluorescence intensity of lucigenin can be described by the Stern-Volmer Equation 1:

$$\frac{I_0}{I_t} = 1 + K_{SV}[Lac^-] \qquad \text{(Equation 1)}$$

where I_0 is the initial fluorescence intensity (i.e., before the addition of the L-lactate solution), I_t the fluorescence intensity at a given time (i.e., after adding aliquots of the L-lactate solution), K_{SV} the Stern-Volmer constant and $[Lac^-]$ the concentration of L-lactate. Therefore, plotting of (I_0/I_t) against $[Lac^-]$ provides K_{SV}. In order to calculate the (I_0/I_t) relationship, data at 503 nm, the wavelength of the maximum of the emission band, were considered. In this case, K_{SV} = 25.4(7) M^{-1} (Figure S90).

Once this titration was performed, experiments with POPC were conducted. 7:3 POPC:cholesterol vesicles were loaded with a $NaNO_3$ aqueous solution (102.2 mM $NaNO_3$, 20 mM NaH_2PO_4, 1 mM lucigenin, I.S. 150 mM, pH 7.2) and treated according to the procedure described previously. Experiments were performed in 1-cm disposable cells, the final POPC concentration in the cuvette being 0.5 mM and the final volume 2.5 mL. Just before starting the measurements, the required volume of the vesicles stock solution was suspended in the outer solution (102.2 mM $NaNO_3$, 20 mM NaH_2PO_4, I.S. 150 mM, pH 7.2) and, at t = 0 s, an aliquot of a 500 mM NaLac aqueous solution prepared with the external solution (102.2 mM $NaNO_3$, 20 mM NaH_2PO_4, I.S. 150 mM, pH 7.2) was added, the Lac^- concentration during the assay being 40 mM. At t = 60 s an aliquot of a solution of the corresponding compound in MeOH (or the blank, MeOH, 1.25 μL) was added, and the emission spectra recorded for five minutes more (excitation wavelength: 372 nm). Finally, the (I_t/I_0) relationship, calculated with the data collected at 503 nm, was plotted against time for each concentration of compound tried.

Biological assays

Cell viability assays

Cytotoxic potential of click-tambjamines was assessed through cell viability experiments using the 3-(4,5-dimethylthiazol-2-yl)-2,5-diphenyltetrazolium bromide (MTT, Sigma-Aldrich, Merck KGaA) colourimetric assay. Cell lines were seeded at 10^4 cell/well in 100 μl using 96-well microtiter plates and were incubated overnight. Next day, cells were treated with experimental compounds at different ranging concentrations (0.8 to 100 μmol/L) or with DMSO as control. After 24 h of compound incubation, 10 μL of MTT solution were added (5 mg/mL) to the plate and incubated for 2 h at 37°C. Then, the medium was removed and formazan crystals were dissolved in 100 μL DMSO. Absorbance was read in a spectrophotometer at 570 nm using a multiwell plate reader (Multiskan FC, Thermo Fisher Scientific Inc.). Cell viability and inhibitory concentration (IC) values of 25%, 50% and 75% of the cell population were calculated using GraphPad Prism 8.0.1 for Windows (Graph-Pad for Science Inc., San Diego, CA, USA). All data are presented as the mean $\pm$ standard deviation (SD) of at least three independent experiments.

Lactate transport experiments

The ability of compound **1** to transport lactate anions across cellular membranes was assessed by measuring both extra- and intracellular lactate levels using a luminescent-based method (Lactate-Glo™ Assay Kit, Promega, WI, USA). This assay couples lactate oxidation and NAD^+ reduction with a bioluminescent NADH detection system. In this reaction, lactate dehydrogenase catalyses lactate conversion into pyruvate with concomitant production of NADH, which is then enzymatically oxidised to convert a pro-luciferin substrate into luciferin. Briefly, HeLa cells were seeded in 12-well plates at 10^5 cells/mL and incubated overnight. Next day, after 60 and 120 min of treatment using IC_{75} value of **1**, medium was collected, cells were washed with PBS and then permeabilised with 150 μL HCl (0.2 M) diluted in PBS 1X for 5 min. Intracellular extracts in HCl were neutralised with 50 μL Tris-base (1 M) before incubation with lactate detection reagent (ratio 1:1). Extracellular lactate levels were measured in the medium previously collected. Luminescence was recorded after 1 h of reaction using a FLUORstar OPTIMA plate reader (BMG LabTech, Ortenberg, Germany) and both extra- and intracellular lactate concentrations determined from a proper standard curve. Lactate levels were normalised to protein content (BCA protein assay kit, PierceTM, Thermo Fisher Scientific Inc.) by lysing cells using SDS (2% v/v) after collecting intracellular extracts. In some conditions, previous to compound addition, monocarboxylate transporters (MCTs) were pharmacologically inhibited using Syrosingopine (Syro, 10 μM, pre-treatment 1 h) to prevent basal lactate shuttle of glycolytic cancer cells. Additionally, **4** and **5** were used as negative controls due to their chemical structural similarity with **1** and their previosly observed low anionphoric activity.

Combination therapy experiments

The potential of **1** to sensitise cancer cells against cisplatin (CisPt) was assessed through MTT cell viability assays. For this, HeLa cells were seeded at 10^4 cell/well in 100 μl in 96-well microtiter plates and incubated overnight. Next day, cells were treated with compound **1** (IC_{10}, IC_{25}, IC_{50} and IC_{75} values) or CisPt as monotherapy or in combination. The combination therapy was performed sequentially by adding compound **1** first and after 24 h CisPt for another 24 h. Cell viability percentages were calculated and plotted using GraphPad Prism 8.0.1 for Windows. The percentages of cell population affected by the combination therapy were analysed with CompuSyn software (version 1.0; ComboSyn Inc., Paramus, NJ, USA) to determine the Combination Index (CI). CI is used to describe the type of interaction between therapeutic compounds that can be synergic ($0.30 < CI < 0.70$), moderate synergic ($0.70 < CI < 0.85$), slight synergic ($0.85 < CI < 0.90$), additive ($0.90 < CI < 1.10$) or antagonist ($CI > 1.10$).

QUANTIFICATION AND STATISTICAL ANALYSIS

Statistical analysis was performed using GraphPad Prism 8.0.1 for Windows (Graph-Pad for Science Inc., San Diego, CA, USA). One-way Anova test was used in biological assays to compare lactate levels between treatments with different compounds. Each experiment was performed at least three times and bars represent mean $\pm$ SEM. One-way ANOVA was performed and statistical differences are indicated as follows: ** $p < 0.01$, *** $p < 0.001$, and **** $p < 0.0001$ for comparison with DMSO; †† $p < 0.01$, and ††† $p < 0.001$ for comparison with Syro.